The Dome Fuji ice core DF2021 chronology (0-207 kyr BP)

Ikumi Oyabu, Kenji Kawamura, Christo Buizert, Frédéric Parrenin, Anais
Orsi, Kyotaro Kitamura, Shuji Aoki, Takakiyo Nakazawa

The Dome Fuji ice core DF2021 chronology (0−207 kyr BP)

Ikumi Oyabu [a, *], Kenji Kawamura [a, b, c], Christo Buizert [d], Frédéric Parrenin [e], Anais Orsi [f, g], Kyotaro Kitamura [a], Shuji Aoki [h], Takakiyo Nakazawa [h]

[a] National Institute of Polar Research, Tokyo, 190-8518, Japan
[b] Department of Polar Science, The Graduate University of Advanced Studies, SOKENDAI, Tokyo, 190-8518, Japan
[c] Japan Agency for Marine Science and Technology (JAMSTEC), Yokosuka, 237-0061, Japan
[d] College of Earth, Ocean, and Atmospheric Sciences, Oregon State University, Corvallis, OR, 97331, USA
[e] Université Grenoble Alpes, CNRS, IRD, Grenoble INP, IGE, 38000, Grenoble, France
[f] Laboratoire des Sciences du Climat et de l'Environnement, LSCE/IPSL, CEA-CNRS-UVSQ, Université Paris-Saclay, Gif-sur-Yvette, France
[g] Earth Ocean and Atmospheric Sciences Department, The University of British Columbia, 2207 Main Mall #2020, Vancouver, BC, V6T 1Z4, Canada
[h] Center for Atmospheric and Oceanic Studies, Graduate School of Science, Tohoku University, Sendai, 980-8578, Japan

ARTICLE INFO

ABSTRACT

Precise ice-core chronologies are essential for identifying the timing and duration of polar climatic changes as well as their phasing with the changes in other parts of the globe. However, existing ice-core chronologies beyond the last 60 kyr show relatively large disagreements with each other and with U−Th chronologies of speleothems. Here, we constructed new ice and gas age scales for the Dome Fuji (DF) core (DF2021) over the last 207 kyr by combining a Bayesian dating model and firn densification model, constrained by various types of chronological and glaciological information including new $\delta O_2/N_2$ age markers, precise synchronization to other high-quality chronologies (volcanic, cosmogenic, and CH_4 signals), and high-resolution $\delta^{15}N$ of N_2 (reflecting past firn thickness). The new chronology is tightly constrained by synchronization to other well-dated records for the last 60 kyr, whereas it is independent from other chronologies for the older period. For the last 60 kyr, the DF2021 chronology agrees with the layer-counted ice core chronologies (GICC05 and a part of WD2014) and U−Th chronologies of speleothems within ~200 years. For the period 60−130 kyr BP, the timing of all Dansgaard-Oeschger warming events on DF2021 agree with those of corresponding events in the U−Th dated Chinese or European speleothems mostly within 1 kyr (well within 2σ uncertainty of DF2021). The excellent agreement suggests high accuracy of our chronology, and supports the assumption of negligible phasing between the past local summer solstice insolation and $\delta O_2/N_2$ fractionation at bubble close-off (the basis for constructing the $\delta O_2/N_2$ age markers). Between 130 and 207 kyr BP (penultimate glacial period), there is a lower degree of similarity between the variations in atmospheric CH_4 and speleothem calcite $\delta^{18}O$ than in the last glacial period, making the age comparison challenging. The comparison of DF2021 with 9 U−Th dates at 7 abrupt events shows the mean difference of −0.2 ± 0.8 kyr, which is within the DF2021 uncertainty (on the order of 1.5 kyr). The DF2021 chronology agrees with the AICC2012 chronology within 2 kyr except between ~103 and 128 kyr BP where AICC2012 is likely too young by up to ~4 kyr. By analyzing the lag between $\delta^{18}O$ of O_2 ($\delta^{18}O_{atm}$) on DF2021 and 65°N summer solstice insolation, the relatively large error in AICC2012 is found to originate in three $\delta^{18}O_{atm}$ age markers assuming a constant lag, which are off by more than 3 kyr. The phasing between $\delta^{18}O_{atm}$ and orbital forcing identified in this study may be useful for future ice core dating, especially where other age constraints are weak or lacking.

© 2022 The Authors. Published by Elsevier Ltd. This is an open access article under the CC BY license (http://creativecommons.org/licenses/by/4.0/).

1. Introduction

Polar ice cores preserve valuable information on past climatic and environmental changes, which allow us to investigate forcings and mechanisms that cause variations in Earth's climate. Precise ice

* Corresponding author.
  E-mail address: oyabu.ikumi@nipr.ac.jp (I. Oyabu).

core chronologies are essential to determine sequences and durations of climatic events as well as to examine the phasing with other paleoclimatic records. Ice cores from high-accumulation-rate sites allow us to construct precise age scales by annual layer counting, which is best for relative ages (i.e., durations). For example, Greenland ice cores have been dated back to 60 kyr BP (before 1950 C.E.) by annual layer counting (GICC05, Vinther et al., 2006; Andersen et al., 2006; Rasmussen et al., 2006; Svensson et al., 2006; Svensson et al., 2008). In Antarctica, the WAIS Divide ice core (WDC) has been dated back to 31 kyr BP also by annual layer counting (WD2014, Sigl et al., 2016). On the other hand, annual-layer counting is not possible for Antarctic ice cores with low accumulation rates (e.g., Dome Fuji, Dome C, Vostok). Thus, the age scales of deep ice cores from low-accumulation sites are typically constructed by combining an ice flow model and an accumulation model whose parameters are constrained with various age markers (e.g., Watanabe et al., 2003b; Parrenin et al., 2004; Parrenin et al., 2007a). Such glaciological chronologies can be modified by a simple age tuning (e.g., Kawamura et al., 2007; Lipenkov et al., 2011) or by statistical adjustments of glaciological variables (e.g., thinning, accumulation rate and lock-in depth) along the depth (e.g., Veres et al., 2013; Bazin et al., 2013; Parrenin et al., 2015; Nakano et al., 2016).

For the deep cores, the age may be constrained by aligning climate proxies, such as water isotopic ratios ($\delta^{18}O_{ice}$ or δD), $\delta^{18}O$ of O_2 ($\delta^{18}O_{atm}$), and CH_4 concentration, to either the orbital precession parameter or northern hemisphere insolation, assuming a constant phasing (Waelbroeck et al., 1995; Shackleton, 2000; Parrenin et al., 2001, 2007b; Ruddiman and Raymo, 2003; Dreyfus et al., 2007; Bazin et al., 2013). Their variations are synchronized to respective targets such as the precession parameter or summer insolation in the northern hemisphere, assuming a constant phasing. In reality, variations in the phasing between orbital parameters and climate are expected and should be considered in uncertainty estimates. In practice, the uncertainty in the phasing of the above proxies with respect to precession is typically assumed to be ±6 kyr (about a quarter of a precession cycle) (Petit et al., 1999; Dreyfus et al., 2007).

The local insolation proxies are the $\delta O_2/N_2$ ratio of trapped air (Bender, 2002; Kawamura et al., 2007; Suwa and Bender, 2008) and total air content (TAC) (Raynaud et al., 2007; Lipenkov et al., 2011). Insolation affects snow metamorphism and grain properties in shallow firn, influencing gas fractionation and porosity during bubble close off (Bender, 2002; Fujita et al., 2009; Kawamura et al., 2004, 2007; Raynaud et al., 2007). In terms of the mechanism of the local insolation control on $\delta O_2/N_2$ variation in the ice sheet, the following hypotheses have been proposed by previous studies. During the bubble close-off process at the base of firn, gas molecules with a small diameter (such as He, Ne, H_2, O_2, and Ar) are preferentially excluded from the freshly formed air bubbles to the open pores, and from there to the atmosphere, by molecular diffusion through ice (e.g., Bender et al., 1995; Ikeda-Fukazawa et al., 2005; Severinghaus and Battle, 2006; Oyabu et al., 2021). Thus, the $\delta O_2/N_2$ of trapped air in the ice sheet is always negative relative to the atmosphere, and the degree of the fractionation is thought to be controlled by physical properties of firn (e.g., layering, porosity, tortuosity, grain size, or other microstructural characteristics), which in turn are controlled by the original physical properties set at the snow surface by the intensity of summer insolation (Bender, 2002; Kawamura et al., 2007; Fujita et al., 2009).

The advantage of the $\delta O_2/N_2$ ratio is that the influence of climatic changes appears to be small in the record. Most notably, the strong ~100-kyr power in the Antarctic climatic records (such as $\delta^{18}O_{ice}$) is absent in the $\delta O_2/N_2$ record, by a possible cancellation of the effects of temperature and accumulation changes (Bender, 2002; Kawamura et al., 2007; Suwa and Bender, 2008). The lack

of climatic signal in the $\delta O_2/N_2$ record makes it an excellent tool for constraining the ice-core chronology, if the assumed phasing relative to insolation holds through time. The phasing between the summer solstice insolation at the drilling site and the $\delta O_2/N_2$ could be assumed zero within the typical synchronization uncertainty of 1−2 kyr (Kawamura et al., 2007; Suwa and Bender, 2008; Lipenkov et al., 2011; Landais et al., 2012).

Two deep ice cores with the length of 2503 m (340 kyr) and 3035 m (720 kyr) were drilled at Dome Fuji in the 1990s and 2000s, which are called the first and second Dome Fuji core, respectively (hereafter DF1 and DF2 core) (Motoyama, 2007; Motoyama et al., 2021; Dome Fuji Ice Core Project Members, 2017). The distance between the two boreholes is 43 m at the surface (Motoyama, 2007), and the depth difference between the cores is up to about 2 m for the studied depth range (Fujita et al., 2015). We briefly review the existing chronologies of the DF ice core.

The first glaciological chronology of the DF1 core was constructed with accumulation history by scaling $\delta^{18}O$ of ice with a modern spatial relationship and a one-dimensional ice flow model (Dansgaard-Johnsen model (Dansgaard and Johnsen, 1969),) whose parameters were constrained with two age tie points from volcanic signals at 97.80 m (2.4 kyr BP) and 1849.55 m (141 kyr BP) (Watanabe et al., 2003a). The age of ice at 2500 m was estimated to be 323 kyr BP. Another glaciological chronology for the DF core was developed using an inverse method to simultaneously constrain five parameters in accumulation and ice flow models (Parrenin et al., 2001) with orbital-scale age constraints over the entire length of the core (precession cycle in $\delta^{18}O_{ice}$) (hereafter DFGT-2003) (Watanabe et al., 2003b). The age of ice at a depth of 2500 m was estimated to be 340 kyr BP. Later, Kawamura et al. (2007) modified the DFGT-2003 chronology by matching the $\delta O_2/N_2$ record to local summer solstice insolation, based on their high correlation originally found in the Vostok core (Bender, 2002), between 80 and 340 kyr BP with relatively small uncertainty (DFO-2006). The gas age of DFO-2006 was based on forward modeling of ice age-gas age difference (Δage) with a firn densification model (Pimienta-Barnola model, Barnola et al., 1991; Kawamura et al., 2003). Subsequently, Parrenin et al. (2007a) constructed an improved glaciological chronology (DFGT-2006) by incorporating improved constraints and models such as 16 age markers including about half of the $\delta O_2/N_2$ tie points (every ~20 kyr), better accumulation estimates using d-excess and oceanic corrections on $\delta^{18}O_{ice}$, and glacial-interglacial ice-thickness variations. A sequential Bayesian approach was also developed to locally modify the prior estimates of unknown parameters in the ice-flow and accumulation models along the core, and applied to the DF1 core with all available $\delta O_2/N_2$ tie points but with the assumption of no glacial-interglacial ice-thickness change (Nakano et al., 2016). For the deep part of the DF2 core (~2500−3028 m), the chronology is based on the synchronization to the Antarctic Ice Cores Chronology 2012 (AICC2012) age scale (Bazin et al., 2013) using isotope matching (Dome Fuji Ice Core Project Members, 2017). For the late Holocene, some parts of the DF chronology can be modified by matching its [10]Be records to tree-ring ^{14}C records (Horiuchi et al., 2008; Miyake et al., 2015, 2019; Kanzawa et al., 2021).

Problems in the existing DF chronologies and the potentials for significant improvements are summarized as the following three points.

(1) The previous DF chronologies were poorly constrained for the last 60 kyr, and it has become possible to synchronize the DF chronology to the age scales with high-resolution and precision.

(2) The DFO-2006 chronology (by matching $\delta O_2/N_2$ data with local summer insolation) was found to have unexpectedly large error at ~90 kyr BP due probably to poor quality of the $\delta O_2/N_2$ data. Also, the assumption of zero phasing between $\delta O_2/N_2$ and local

summer insolation has been questioned. The latest high-quality $\delta O_2/N_2$ data by Oyabu et al. (2021) has the potential to solve these problems.

(3)The age scales of the ice and gas were estimated independently for all previous DF chronologies. Probabilistic dating methods have been developed to simultaneously produce coherent ice and gas age scales.

First, the previous DF chronologies were poorly constrained for the last 60 kyr because they relied on only two age markers: one in the late Termination I, and one at the Laschamp geomagnetic event. In this range, it has become possible to synchronize the DF ice age to layer-counted ice cores and tree rings using common signals such as volcanic signals and cosmogenic radionuclides (Horiuchi et al., 2008; Fujita et al., 2015; Buizert et al., 2018; Svensson et al., 2020). Also, high-resolution CH_4 concentration data have been acquired (Oyabu et al., 2020; this study) and available for gas age matching to the WDC and Greenland cores for strong empirical constraints on the Δage.

The second point is related to the $\delta O_2/N_2$ age constraints for the old periods. The $\delta O_2/N_2$ record and local summer insolation is assumed to be synchronous (i.e., zero lag for the alignment, Kawamura et al., 2007), and the uncertainty of DFO-2006 only includes the matching uncertainty due to data scatter and the interpolation uncertainty, to be mostly smaller than ± 2.5 kyr. The DFO-2006 was validated at 4 horizons at 92.6 (volcanic), 103.1 (CH_4), 109.5 (CH_4) and 130.8 (CH_4) kyr BP, by comparing them with radiometric ages of a volcanic eruption and three abrupt shifts in speleothem records. However, it was pointed out from detailed volcanic matching of the DF core to the EPICA Dome C (EDC) ice core, which in turn was dated with U−Th chronology of Chinese speleothems by assuming bipolar seesaw (Barker et al., 2011), that DFO-2006 around 90 kyr BP is too old by ~3 kyr (Fujita et al., 2015). A possible source of this age error is the error of $\delta O_2/N_2$ peak positions because of the large noise (or scatter) in the previous DF $\delta O_2/N_2$ record between 60 and 160 kyr (Kawamura et al., 2007). The large noise may have two possible causes: strong gas loss during core storage, and strong gas fractionation between bubbles and clathrate hydrates (Ikeda-Fukazawa et al., 2005; Oyabu et al., 2021). The more recent $\delta O_2/N_2$ records from the EDC ice core between 100 and 800 kyr (Landais et al., 2012; Bazin et al., 2016; Extier et al., 2018) also showed a large scatter around the orbital-scale variations in some periods, and did not allow one to find consistent relationship with local summer insolation for precise dating. The $\delta O_2/N_2$ records from the EDC, Vostok and DF cores around the last interglacial period (~100−160 kyr BP) also show site-specific high-frequency variability, obscuring the tuning tie points and potentially challenging the assumption of zero phasing between $\delta O_2/N_2$ and local summer insolation (Bazin et al., 2016). However, most of these $\delta O_2/N_2$ data may be significantly affected by post-coring gas loss, thus a reliable assessment of $\delta O_2/N_2$ as a local insolation proxy needs much improved $\delta O_2/N_2$ data with little post-coring gas loss.

A recent study by Oyabu et al. (2020) revealed that the original $\delta O_2/N_2$ signal (not altered by post-coring gas loss) is preserved in the center of the DF core, which has been stored at -50 °C for ~20 years. Using more extensive trimming of ice samples, Oyabu et al. (2021) obtained an $\delta O_2/N_2$ record with little noise that has high similarity to the local summer insolation curve for 90−173 kyr BP. These studies raised the possibility of assessing and improving the age scales by providing precise $\delta O_2/N_2$ age markers.

The third point is related to the coherency of ice and gas age scales. So far, for the DF core, both the methods of Parrenin et al. (2007a) and Nakano et al. (2016) deal with the ice age only, and the Δage (thus gas age) was independently estimated by a forward firn densification model (Barnola et al., 1991). The densification model produces thicker firn in the glacial periods than in the

interglacial periods, which contradicts the evidence from $\delta^{15}N$ of N_2 that suggests a thinner glacial firn column, as well as the depth difference between ice and air with the same age (Δdepth) for the last glacial period (Parrenin et al., 2012; Buizert et al., 2021).

On the other hand, probabilistic dating methods have been developed to optimize the prior estimates of accumulation rate, thinning and lock-in depth (LID, the depth in firn where vertical air diffusion stops) as functions of depth for several ice cores, by integrating various chronological information, to simultaneously produce a common ice and gas age scales (e.g., Datice by Lemieux-Dudon et al., 2010; Icechrono by Parrenin et al., 2015; Paleochrono by Parrenin et al., 2021). The AICC2012 is a common ice and gas age scale constructed for five ice cores (EDC, Vostok, EDML, TALDICE, and NGRIP) using the Datice tool (Bazin et al., 2013; Veres et al., 2013).

Advances in firn densification models now reproduce the thinner glacial firn thickness on the East Antarctic plateau (Bréant et al., 2017; Buizert et al., 2021). The Bréant model reduced its sensitivity at low temperatures and introduced the hypothetical influence of impurities in softening the firn, which enhanced densification rates at cold stages. On the other hand, borehole thermometry suggests that the magnitude of surface temperature cooling during the last glacial maximum was only around $4-5$ °C in interior East Antarctica (Dome Fuji, Dome C), which is less than previous estimates of around $8-10$ °C (Buizert et al., 2021); conventional firn densification models (e.g., Herron-Langway model) could reproduce the thinner glacial firn column using this forcing. Buizert et al. (2021) developed an inverse method with the firn densification model, where an automated routine finds the temperature and accumulation rate that fit the modeled $\delta^{15}N$ and Δage to the ice-core data.

Because the probabilistic dating methods (such as Datice and PaleoChrono) may produce physically unrealistic solutions (such as too rapid changes in firn thickness and gas age reversals) if used with incorrect parameters, they could ideally be combined with the densification models. Also, the probabilistic methods can optimize the accumulation rate, thinning function and LID at high resolution along depth to pass through the given age constraints, thus the accuracy of age markers from ice core data are particularly important.

In this paper, we construct precise and coherent ice and gas time scales of the DF core over the last 207 kyr (0−2150 m), by iterating between the Paleochrono probabilistic dating model (Parrenin et al., 2021) and the inverse Herron-Langway densification model (Buizert et al., 2021) with various types of constraints, including new $\delta O_2/N_2$ ice age markers, CH_4 gas age markers, and $\delta^{15}N$ for firn properties, obtained by recent precise gas measurement on the DF core (Oyabu et al., 2020, 2021), as well as published tie points between the [10]Be flux record in the second DF core and tree-ring ^{14}C record (Horiuchi et al., 2008; Miyake et al., 2015, 2019; Kanzawa et al., 2021). Also, a new volcanic matching of the DF to WDC, and indirectly to NGRIP core (Svensson et al., 2020) were made. We examined the sensitivity of the DF chronology to different sets of priors of accumulation rate, thinning and LID, including the LID from another firn densification model (Bréant model). The constructed chronology was validated by comparing with the U−Th chronologies of speleothems. This study limits the construction of the new age scale to 2150 m because of the currently insufficient resolution and quality of the gas data (CH_4, $\delta O_2/N_2$, and $\delta^{15}N$) for the deeper part, which will be improved in the near future. We note that all ages in this paper and the dataset are reported relative to 1950 C.E.

2. Methods

2.1. General strategy for DF core dating

For the last 60 kyr, we fully utilize the constraints on the ice age and gas age by matching the DF core data (volcanic signals, ^{10}Be and CH$_4$) with the volcanic signals and CH$_4$ of the layer-counted chronologies of high-accumulation ice cores (WD2014 of WDC and GICC05 of Greenland cores) as well as the tree ring ^{14}C. More specifically, the DF ice age intervals (the age difference between two volcanic layers) are constrained by WD2014 for 0−31.2 kyr BP (164 intervals) where WD2014 is determined by the layer counting (Sigl et al., 2016). Also, the DF ice age at 16 layers (^{10}Be peaks) for 0.13−7.4 kyr BP are constrained by tree-ring chronologies through ^{10}Be−^{14}C matching (Horiuchi et al., 2008; Miyake et al., 2015, 2019; Kanzawa et al., 2021). For the gas age, we match the DF and WD CH$_4$ records and NGRIP $\delta^{18}O_{ice}$ records at Dansgaard−Oeschger (DO) events or other transitions. On the other hand, for the period older than 60 kyr BP, we only use the constrains on the ice age from the DF $\delta O_2/N_2$ data and ice depth-gas depth difference (Δdepth) from the DF $\delta^{18}O_{ice}$ and CH$_4$ data, and thus the resulting chronology is independent of other chronologies such as U−Th chronologies of speleothems (e.g., Cheng et al., 2016) and AICC2012 (Veres et al., 2013; Bazin et al., 2013). We derive Δdepth based on the concept of the "thermal bipolar seesaw" (Crowley, 1992; Stocker and Johnsen, 2003), in which a peak in the Antarctic $\delta^{18}O_{ice}$ is assumed synchronous with an abrupt increase in CH$_4$ (Parrenin et al., 2012). See details of the chronological constraints in section 2.4.

An inverse dating method by a probabilistic model with reasonable priors (initial conditions with uncertainties) is best suited for integrating all kinds of age constraints and derives a continuous ice-core chronology. However, probabilistic models may produce a physically unrealistic solution (such as too-rapid changes in firn thickness and resulting gas age reversals, Veres et al., 2013; Bazin et al., 2013) if used with inappropriate parameters. To overcome this potential issue and obtain the best estimates of chronology and associated glaciological parameters, we combine the probabilistic dating model with a firn densification model (Buizert et al., 2021), as follows.

2.2. Models

The age of ice ($\chi(z)$) and gas ($\psi(z)$) of an ice core can be described by accumulation rate (A), lock-in depth (LID) (the depth in firn where air is effectively isolated from the overlying atmosphere), and thinning function (the ratio of a thickness of an ice layer to the initial accumulation at the surface) (τ), as follows:

$$\chi(z) = \chi_0 + \int_{z_0}^{z} \frac{D(z')}{A(z')\tau(z')} dz' \tag{1}$$

$$\psi(z) = \chi(z - \Delta\text{depth}(z)) \tag{2}$$

$$\int_{z-\Delta_{\text{depth}}(z)}^{z} \frac{D(z')}{\tau(z')} dz' = l(z) \times \frac{D}{\tau}\Big|_{firn}^{0} \tag{3}$$

where z is the depth along with the ice core record, χ_0 is the age of the ice at the top (with depth $z = z_0$), D is the relative density of the snow to ice (dimensionless), Δdepth is the depth difference between gas and ice of the same age, and l is the lock-in depth of air

bubbles and $\frac{D}{\tau}\big|_{firn}^{0}$ is the average value of $\frac{D}{\tau}$ in the firn when the air particle was at the lock-in-depth. To find the best chronology, we use the software for automated optimization of paleoclimatic chronologies *Paleochrono* (Parrenin et al., 2021). In the case of its application to ice cores, Paleochrono is equivalent to its predecessor IceChrono (Parrenin et al., 2015), but with computing time improvements. It optimizes A, LID and τ along depth using various chronological constraints such as absolute age horizons, age difference between two depths (age intervals), and Δdepth. The chronological constraints are derived from volcanic and CH$_4$ matching to other well-dated cores, ^{10}Be matching to tree-ring ^{14}C records, comparison of $\delta O_2/N_2$ with insolation, and climatic synchroneity in northern and southern hemispheres for $\delta^{18}O$ (ice) and CH$_4$ (gas) depths (see 2.5). They are combined using a Bayesian framework to obtain a posterior estimate of the unknown variables (A, LID and τ) and the resulting chronology with uncertainties.

To estimate the priors of A and LID, we used the dynamical firn densification-heat transport model (DynaDens model, Buizert et al., 2021 and references therein) based on the overburden-pressure formulation of the Herron-Langway firn model (Herron and Langway, 1980, Equation 4c). The model is run in an inverse mode, where an automated routine is used to find the temperature (T_{site}) and accumulation rate (A) that optimize the fit to δ^{15}N and Δage data. Past accumulation rates are uniquely constrained by the combination of δ^{15}N and Δage (Buizert, 2021). The following model parameters were used: a surface density of 335 kg m^{-3}; a convective zone thickness of 4 m (Kawamura et al., 2006); a lock-in density that is 3 kg m^{-3} lower than the bubble close-off density by Martinerie et al. (1994); and a critical density of 540 kg m^{-3} rather than the standard 550 kg m^{-3} (to improve the fit to density measurements at the site). The initial guesses of T_{site} and A are derived from linear scaling of the site temperature record by Uemura et al. (2018), which we shall call $T_{initial}$.

Our inverse method results in a temperature history T_{site} with a small magnitude (~4 °C) of surface cooling during the last glacial maximum; while in agreement with Dome Fuji borehole-thermometry reconstructions (Buizert et al., 2021). The result is currently under discussion as other studies have inferred much lower LGM temperatures at the DF site (and other East Antarctic inland cores) based on stable water isotopes (e.g., Sime et al., 2009; Uemura et al., 2018). One can think of the firn model as a physically-consistent way to interpolate between the empirical Δage estimates. Combined, the δ^{15}N and Δage data constrain past accumulation rates and firn densification rates. Here we achieve the required past densification rates by implementing a ~4 °C glacial cooling, but it remains conceivable that the required densification rates can also be achieved with strongly altered description of firn densification physics and a ~15 °C glacial cooling (see section 3.2). Any firn densification description that can fit the δ^{15}N and Δage data will result in similar histories of past accumulation and LID, and the DF chronology we reconstruct is to first order independent of assumptions regarding the magnitude of glacial cooling. In this paper we remain noncommittal on the magnitude of glacial cooling.

To bring A and LID as estimated by Paleochrono and DynaDens in agreement with each other, we employ an iterative approach between the Paleochrono and DynaDens models with the following steps.

Step 1: Construct initial scenarios of A and τ using a one-dimensional ice flow model (Parrenin et al., 2007a), and LID using δ^{15}N data corrected for thermal signal (Buizert et al., 2021) (see 2.4).

Step 2: Run Paleochrono with the priors from Step 1 and various age constraints (see 2.5) to produce a tentative age scale of ice and gas, together with revised glaciological parameters (A, LID and τ).

Step 3: Revise the $\delta O_2/N_2$ control points and Δdepth (see 2.5.2), and deduce Δage for the depths where Δdepth are available (see 2.5.5), using the age scale from Step 2.

Step 4: Run DynaDens in the inverse mode to find linear scaling factors for T_{site} and A from the initial $T_{initial}$ (Uemura et al., 2018) that optimize the Δage (from Step 3) and $\delta^{15}N$ for the last 50 kyr.

Step 5: Run DynaDens in the forward mode using the optimized T_{site} and A from Step 4 to construct the history of Δage over the whole 207 kyr age range (base run).

Step 6: Let DynaDens change T_{site} and A simultaneously and independently to improve the fit of $\delta^{15}N$ for all times older than 50 kyr BP, while forcing the model to match the Δage history from the base run.

Step 7: Let DynaDens change T_{site} and A simultaneously and independently to improve the fits of both the $\delta^{15}N$ and Δage data for the last 50 kyr.

Step 8: Revise the $\delta^{15}N$-based LID by subtracting modeled thermal component of $\delta^{15}N$ from Step 7 from the $\delta^{15}N$ data.

Step 9: Run Paleochrono with A from Step 6 and 7, LID from Step 8, τ from Step 2, $_2$ control points from Step 3 to revise the ice age, gas age, A, LID and τ.

The ice and gas age scales from Step 9 agree with those from Step 2 within 400 years, thus, only one iteration is needed.

It is necessary to give uncertainties for the priors of A, τ and LID for Paleochrono. We assigned the uncertainty of A as 25% (1σ) for Step 2 (1st run of Paleochrono) and 20% (1σ) for Step 9 (2nd run of Paleochrono). The uncertainty of the Antarctic A converted from stable water isotope is typically ~20% (Parrenin et al., 2007a), and we assigned 25% for Step 2 as a conservative number. The uncertainty of τ is difficult to assess, but it seems reasonable to assume that the uncertainty increases with depth. Thus, we assigned it by linear interpolation between the ice-sheet surface (0%) and the bottom (100%) (1σ) with depth, as a first approximation for Step 2. We also set a stiffness parameter for τ ($\lambda_{thinning} = 6000$) to make it monotonically decrease with depth. For the uncertainty of τ in Step 9, we employed the error estimate by Paleochrono in Step 2 (ranging $0-3.5\%$, 1σ), with $\lambda_{thinning}$ of 250. We assigned 5% (1σ) for the uncertainty of LID in both Step 2 and Step 9, because the LID estimated with two firn densification models (DynaDens and Bréant models) and $\delta^{15}N$ data (Step 1) mostly agree within 5% of each other.

To examine whether the chronology after Step 9 (Paleochrono) is sensitive to the prior of LID used in the intermediate steps, we tested the method with another firn densification model (Bréant model, Bréant et al., 2017). We conducted an experiment using the thermal component of $\delta^{15}N$ from Bréant model, as well as experiments skipping Step 8 and using the LID from DynaDens and Bréant model in Step 9 directly. Details are described in section 3.2.

We note that an assumption of Paleochrono is that all prior information on A, τ and LID, and age constraints are independent, which is not the case in our approach with the iteration between Paleochrono and DynaDens. Ideally, Paleochrono would be coupled with DynaDens and invert both at the same time, which would be a future direction towards an improved method.

2.3. Dome Fuji ice core data

We used newly measured and published datasets to establish the age constraints and model inputs (Table 1). New measurements and synthesizing of different datasets (measured at different institutes) are explained in the following sections.

2.3.1. CH₄ concentration

We used three datasets of CH_4 (Fig. 2b). The first dataset was generated at National Institute of Polar Research (NIPR) by new measurements of the DF1 ice core. The detailed measurement method is described elsewhere (Oyabu et al., 2020). Briefly, an ice sample of ~60 g was evacuated for 2 h and melted, and the released air was cryogenically collected into a sample tube. The air sample was split into two aliquots and measured with gas chromatographs (two Agilent 7890A, for CH_4, N_2O and CO_2 concentrations) and a mass spectrometer (Thermo DELTA V, for $\delta O_2/N_2$, $\delta Ar/N_2$, $\delta^{15}N$ and $\delta^{18}O$). We measured 595 and 219 samples with single and replicates (in total 814 samples), respectively, between 112.88 and 2148.62 m, with an overall precision of better than ~3 ppb.

The second data set was generated at Tohoku University (TU) (Kawamura, 2001). A total of 222 samples from 120.19 to 2144.62 m were measured with the overall precision of ~6 ppb. The raw data were corrected for systematic negative bias (presumably by selective adsorption of CH_4 on the inner walls of apparatus) by $+1.1$ $- +3.2$ ppb, based on the results of blank tests and CH_4 concentration of each sample. The corrected data did not show systematic differences from the newest data measured at NIPR (this study). $\delta^{15}N$ was also measured for each sample.

The CH_4 concentrations at NIPR and TU were determined on the TU concentration scale (Nakazawa et al., 1993; Oyabu et al., 2020) and corrected for the gravitational enrichment in firn using the measured $\delta^{15}N$ (Sowers et al., 1989).

The third dataset was from the measurements at Institut des Géosciences de l'Environnement (IGE) with the overall precision of ~10 ppb, as published by Buizert et al. (2021). This dataset had an offset from the NIPR/TU datasets probably due to different calibration scales. We added 23.5 ppb to the IGE data to account for the different calibration scale and gravitational correction.

We used all NIPR CH_4 data because it has the highest precision, and added the data from the other two datasets to increase the resolution. We excluded some of the TU and IGE data points according to these criteria: (1) they are close to the neighboring NIPR data points on both sides ($\sim< 100$ yr) with large differences (>10 ppb) (53 points in $0-28$ kyr BP and one point at 140 kyr BP), (2) the additional data produce false CH_4 peaks in comparison to the high-precision WAIS Divide data (Rhodes et al., 2015) (17 points in $28-65$ kyr BP), or (3) the additional data produce a marked negative spike in MIS 6 which appears artificial in comparison with the record in the last glacial period (one point at 189 kyr BP) (Fig. A1). We note that the outlier rejections as above are intended for completeness of the high-quality CH_4 record, but they do not affect the positions of the age control points.

2.3.2. $\delta O_2/N_2$ and $\delta^{15}N$

We measured $\delta O_2/N_2$ and $\delta^{15}N$ between 2003.38 and 2157.56 m ($171-207$ kyr BP in gas age) using an established method (Oyabu et al., 2020, 2021) at 54 and 14 depths with single and replicates, respectively (mostly with CH_4 concentrations). The gravitational corrections for $\delta O_2/N_2$ data are made using the $\delta^{15}N$ data of the same samples (Oyabu et al., 2020). We combined the new data with the previous dataset.

2.4. Initial scenarios of A, τ, and LID (in step 1)

An inverse method using one-dimensional ice-flow and accumulation models (Parrenin et al., 2007a) was employed to obtain the initial scenarios of A and τ. The model optimizes five parameters in the ice flow and accumulation models to reproduce the given age markers. The input data for the models are $\Delta T_{initial}$ (Uemura et al., 2018), which was scaled to A in the accumulation model, and absolute ice-age markers based on the ^{10}Be and $\delta O_2/N_2$ data for the last 207 kyr BP (see 2.5.2), added by published age markers for the older period (Dome Fuji Ice Core Project Members, 2017). The initial scenario of LID was constructed by converting the

Table 1
Dome Fuji ice core data.

Species	Depth range (m)	Reference	Remarks
CH_4	112.88−2148.62	This study, Oyabu et al. (2020)	Measured at NIPR in 2015−2021
CH_4	120.19−2144.62	Kawamura (2001)'; Buizert et al. (2021)	Measured at TU in 1999−2000
CH_4	413.89−937.08	Buizert et al. (2021)	Measured at IGE in 2010
$\delta O_2/N_2$	112.88−2148.62	This study, Oyabu et al. (2020), Oyabu et al. (2021)	
$\delta^{15}N$	112.88−2148.62	This study, Oyabu et al. (2020), Oyabu et al. (2021), Buizert et al. (2021)	
$\delta^{18}O_{ice}$	1.63−2158.0	Dome Fuji Ice Core Project Members. (2017)	Sawdust samples
ΔT_{site}	1.63−2158.0	Uemura et al. (2018)	
ECM	6.2−1020	Fujita et al. (2015)	
$^{10}Be-^{14}C$ matching	8.5−241.94 (DF2001 and DF2 core)	Horiuchi et al. (2008), Miyake et al. (2015), Miyake et al. (2019), Kanzawa et al. (2021)	DF2001 or DF2 core, converted to DF1 core depth

gravitational component of $\delta^{15}N$ data ($\delta^{15}N_{grav}$) with a barometric equation ($\delta^{15}N_{grav} \approx \Delta mgz/RT \times 1000$, in ‰) (Schwander, 1989), where Δm is mass difference, g is the gravitational acceleration, z is the thickness of diffusive layer in firn (LID minus convective zone thickness), R is the ideal gas constant, and T is temperature. $\delta^{15}N_{grav}$ was deduced by subtracting thermal component ($\delta^{15}N_{therm}$) from the measured $\delta^{15}N$ record (Severinghaus et al., 1998). For the initial scenario, we assumed a constant $\delta^{15}N_{therm}$ (= −0.026‰), which was the average of published values over 2.5−54 kyr BP from the DynaDens model (Buizert et al., 2021), and a constant convective zone (4 m) (Buizert et al., 2021; Kawamura et al., 2006). To reduce short-term scatters in the original $\delta^{15}N$ record, we slightly smoothed the record by the three-point running mean, evenly resampled at 0.1-kyr intervals, and smoothed it by the 0.7-kyr running mean (Fig. 1). We estimated the uncertainty of LID as 5% (1 σ) based on the discrepancy between $\delta^{15}N$-based LID and DynaDens LID.

2.5. Age constraints

#### 2.5.1. Intervals between neighboring ice age markers (ice age intervals)

We take advantage of the ability of the Paleochrono model to accommodate age differences between stratigraphic layers (ice age intervals) with uncertainties as the age constraints (Parrenin et al., 2015). This type of constraints is suitable for incorporating the layer-counted part of the WAIS Divide age scale (WD2014) into the DF chronology through volcanic synchronization (0−31.2 kyr BP). Previous works synchronized between the WD and EDC cores

(Buizert et al., 2018), and between the DF and EDC cores (Fujita et al., 2015), but the direct synchronization between the DF and WD cores was lacking. Thus, using the indirect synchronization between the DF and WD cores from the previous studies as a guide, we newly identified common volcanic peaks between the ECM of the DF core (Fujita et al., 2015) and sulfur (or SO_4^{2-}) concentrations of the WD core (McConnell, 2017; Cole-Dai et al., 2014a, 2014b). The matchings were independently conducted by two investigators (I. Oyabu and K. Kawamura), and the common picks (167 tie points) were employed. We note that the DF core can also be precisely synchronized to the Greenland Ice Core Chronology (GICC05) via the bipolar volcanic matching between the NGRIP and WD cores by Svensson et al. (2020) (Supplemental data). The volcanic synchronization between the DF and NGRIP cores is used for Δdepth estimates (see section 2.5.4) (thus, not used for the ice age intervals or absolute ice age markers).

From the WD-DF tie points, 165 ice age intervals are derived, most of which are smaller than 300 years (maximum is about 2000 years). The uncertainty of ice age interval has two components: (1) counting uncertainty in the original WD2014 age scale for the intervals (0.1−10.6 years, larger for the deeper depth) and (2) depth uncertainty for matching between the two cores (<2 years, associated with data resolution). Total uncertainty of the ice age interval is estimated to be 0.1−10.8 years (one standard deviation).

2.5.2. Absolute ice age markers

For the last 7500 years (11−242 m), we use the published tie points between the ^{10}Be flux record in the second DF core and tree-ring ^{14}C record (Horiuchi et al., 2008; Miyake et al., 2015, 2019,
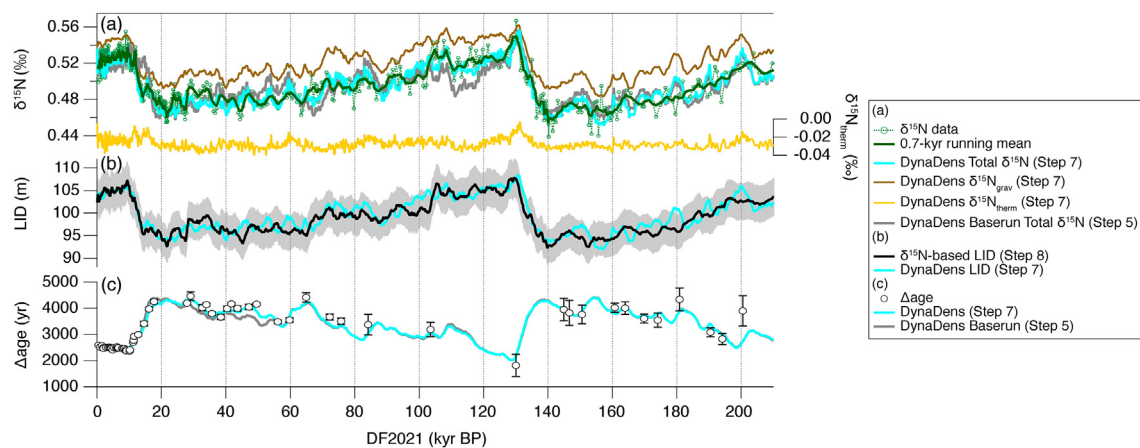
Fig. 1. Comparisons of data and model for $\delta^{15}N$, LID and Δage of the DF core. (a) $\delta^{15}N$ data and its 0.7-kyr running mean, modeled $\delta^{15}N$ (total as well as gravitational and thermal components) from the DynaDens model in inverse mode (Step 7), and modeled total $\delta^{15}N$ from the DynaDens model but with linear scaling factors for temperature and accumulation rate (base run, Step 5). (b) LID by subtracting modeled $\delta^{15}N_{therm}$ from smoothed $\delta^{15}N$ data, and that by DynaDens model (Step 7). Grey shading indicates the estimated uncertainty (1 σ) for the $\delta^{15}N$-based LID. (c) Empirical and modeled Δage (model results are after Step 5 and Step 7 by DynaDens model).
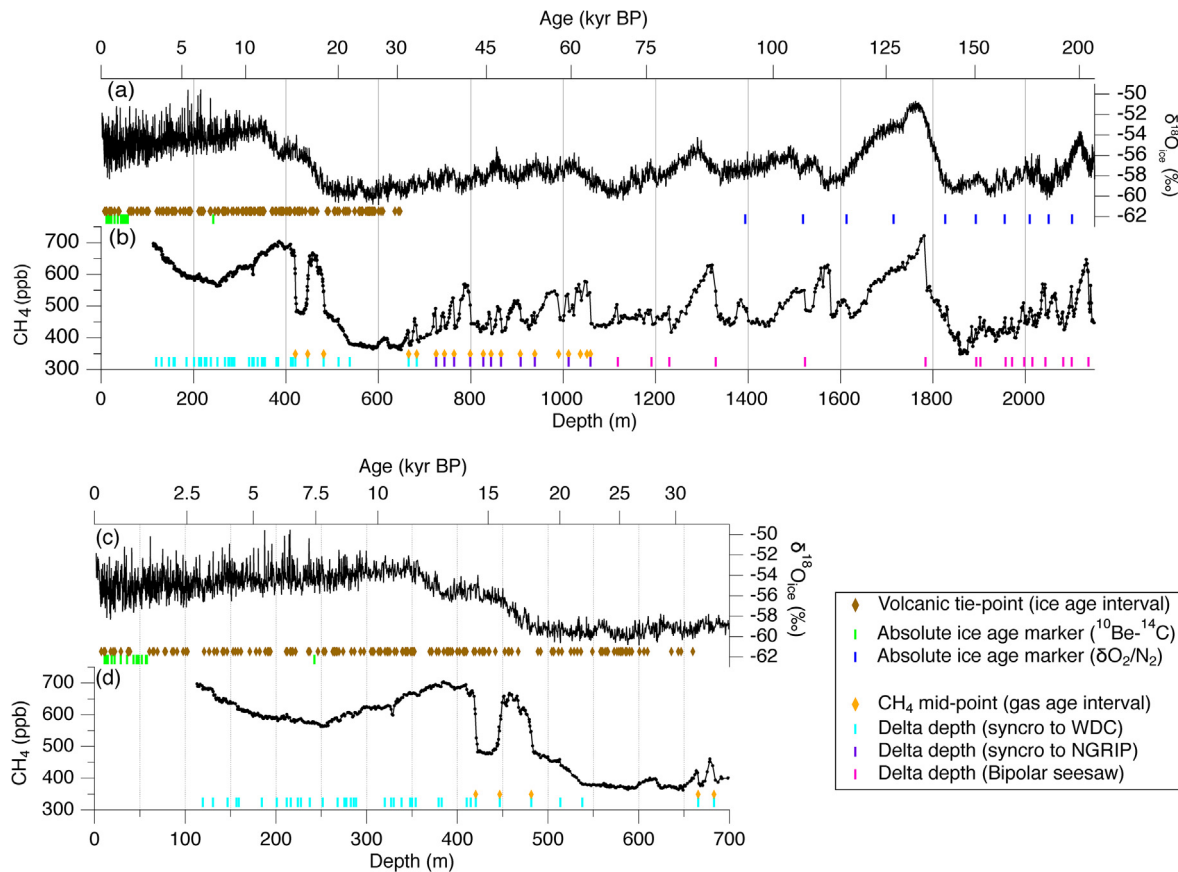
Fig. 2. Age constraints for ice and gas in the DF core. (a) Ice age constraints with $\delta^{18}O_{ice}$ as reference (Dome Fuji Ice Core Project Members, 2017). Different markers indicate the volcanic horizons for intervals between neighboring ice age markers (ice age intervals), ^{10}Be absolute age markers, and $\delta O_2/N_2$ age markers. (b) Gas age constraints with CH_4 record as reference. Different markers indicate the CH_4 transitions (for DO events and minor wiggles) for deducing intervals between neighboring gas age markers (gas age intervals) or Δdepth through the synchronization to WDC or NGRIP core (for 0–65 kyr BP), or through bipolar-seesaw assumption (>65 kyr BP). (c) and (d) Enlarged views of (a) and (b), respectively.

Table 2
Absolute ice age markers from matching of ice-core ^{10}Be with tree-ring ^{14}C.

Ice depth (m, DF1)	Ice age (yr before 1950)	1σ (yr)	Core name	Reference
11.07	135	4.26	DF2001	Horiuchi et al. (2008)
12.59	165	4.26	DF2001	Horiuchi et al. (2008)
14.60	195	4.26	DF2001	Horiuchi et al. (2008)
18.90	265	5.02	DF2001	Horiuchi et al. (2008)
22.00	345	4.02	DF2001	Horiuchi et al. (2008)
28.90	505	4.22	DF2001	Horiuchi et al. (2008)
35.90	645	5.15	DF2001	Horiuchi et al. (2008)
43.00	805	5.87	DF2001	Horiuchi et al. (2008)
46.30	905	5.70	DF2001	Horiuchi et al. (2008)
47.60	935	5.43	DF2001	Horiuchi et al. (2008)
48.47	956	0.78	DF2001	Miyake et al. (2015)
52.10	1045	5.35	DF2001	Horiuchi et al. (2008)
56.70	1165	6.88	DF2001	Horiuchi et al. (2008)
56.81	1175	1.01	DF2001	Miyake et al. (2019)
57.60	1195	6.88	DF2001	Horiuchi et al. (2008)
242.37	7427	2.65	DF2	Kanzawa et al. (2021)

Kanzawa et al., 2021, Table 2). We converted the depths of DF2001 core (the shallow part of the second DF core) and the second DF core (DF2), on which ^{10}Be was measured, to the depths of the first DF core using the published volcanic signals (Motizuki et al., 2014; Fujita et al., 2015). The total age uncertainty of the absolute age at the ^{10}Be peaks are 0.8–7 years (1σ), which is the combination of the matching error (0.6–7 years, depending on the DF data resolution) and the depth conversion error (0.02–0.03 m, corresponding to

0.3–0.6 years).

For the period older than ~90 kyr BP, we use orbital control points between $\delta O_2/N_2$ and local insolation (Fig. 3 and Table 3; Oyabu et al., 2021 and this study). Oyabu et al. (2021) confirmed close similarity between the summer solstice insolation at 77°S and $\delta O_2/N_2$ in the DF core for the period older than ~90 kyr BP by high-precision measurements. For the period younger than ~90 kyr BP, they found large scatter in the $\delta O_2/N_2$ data in the lower part and
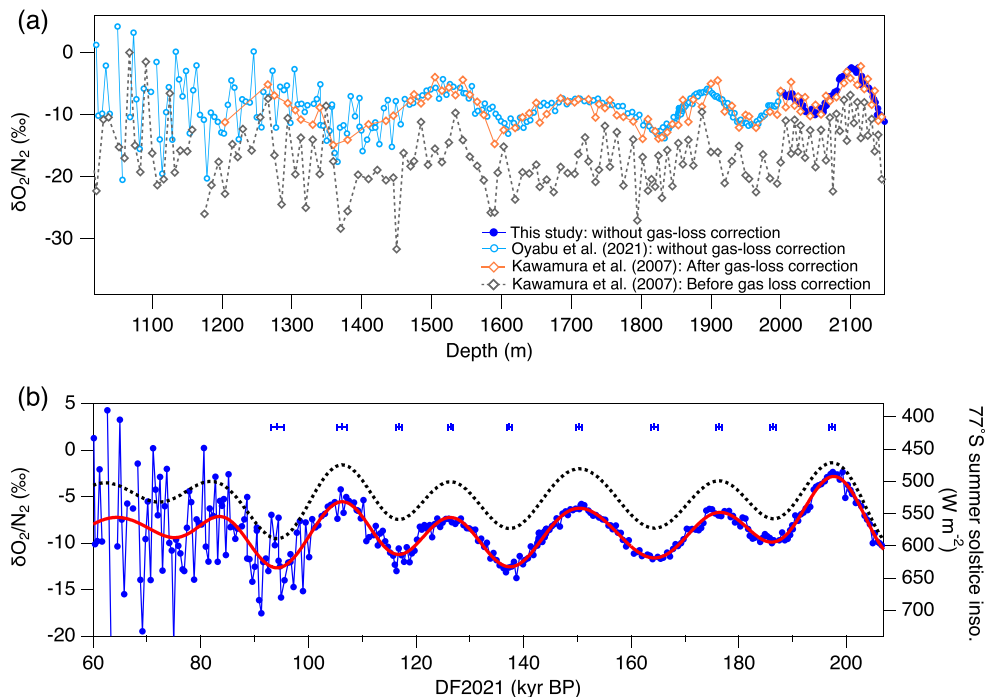
Fig. 3. $\delta O_2/N_2$ from the DF core. (a) Comparison of the new $\delta O_2/N_2$ data used for the DF2021 chronology (Oyabu et al., 2021 and this study) with the previous data for the DFO-2006 chronology (Kawamura et al., 2007) from the DF core. While the previous data were treated by post-coring gas-loss correction and outlier rejection, the correction was not necessary for the new data because of improved sample treatment and measurement. (b) New $\delta O_2/N_2$ data (blue circles), low-pass filtered $\delta O_2/N_2$ record for identifying age markers (red line), summer solstice insolation at 77°S (black dotted line; computed with the Analyseries software, Paillard et al., 1996 with solution of Laskar et al., 2004), and peak ages in the filtered $\delta O_2/N_2$ with 2σ uncertainty used as age markers for DF2021 (blue markers with error bars at the top). (For interpretation of the references to colour in this figure legend, the reader is referred to the Web version of this article.)

Table 3
Absolute ice age markers from $\delta O_2/N_2$.

Ice depth (m)	Age (yr BP)	1σ (yr)
1393.91	94184	588
1518.57	106243	417
1612.87	116814	258
1714.79	126404	251
1826.35	137372	252
1892.60	150331	284
1955.20	164315	287
2009.24	176283	271
2050.12	186408	250
2100.89	197314	229

just below the bubble-clathrate hydrate transition zone (BCTZ). In the BCTZ, extreme gas fractionation on the order of several hundreds of ‰ occur between individual bubbles and clathrate hydrates (Ikeda-Fukazawa et al., 2001). This process also fractionates $\delta O_2/N_2$ between mm-scale layers in the ice sheet, causing the large scatter in the $\delta O_2/N_2$ data. In the DF core, this transition is completed at ~1200 m depth (~77 kyr BP), and the scatter becomes smaller with depth until it is negligible at ~1500 m (~100 kyr BP) because of gradual smoothing by molecular diffusion between the layers (Lüthi et al., 2010; Oyabu et al., 2021). See Oyabu et al. (2021) for details. We used the ages of maxima and minima in the $\delta O_2/N_2$ record as the synchronization tie points, which are assumed to be synchronous with the peaks in the summer solstice insolation. To identify the ages of maxima and minima in the $\delta O_2/N_2$ record on the orbital-scale timescale, the $\delta O_2/N_2$ data was first put on the DFGT-2003 chronology (Watanabe et al., 2003b), linearly interpolated at 0.1 kyr intervals and smoothed with the low-pass filter (cut-off period: 16.7 kyr; Kawamura et al., 2007). The maxima and

minima in the smoothed $\delta O_2/N_2$ record were used as the control points and used for Step 1. As the chronology was revised after Step 1, the maxima and minima in the $\delta O_2/N_2$ were re-calculated and used as the control points for Step 2.

We assume no lag of the $\delta O_2/N_2$ record behind summer solstice insolation, following the discussion of Kawamura et al. (2007). Briefly, the seasonal maximum of air temperature at DF lags the insolation maximum by ~1 week (Fig. A2), roughly corresponding to an age offset of ~500 years if the snow properties responsible for the ice-core $\delta O_2/N_2$ signals varies synchronously with air temperature. However, the actual lag of the changes of snow properties behind insolation is expected to be smaller, considering that solar energy should also be directly absorbed by the near-surface snow and affects its properties, and that the seasonal maximum in the vertical temperature gradient (between 10 and 50 cm depths) is observed slightly earlier than the summer solstice (Kawamura et al., 2007). Also, as discussed below, our new DF O_2/N_2 chronology agrees well with the U−Th chronologies of Chinese and European speleothems within their uncertainties, supporting the assumption of zero lag.

The uncertainty of the $\delta O_2/N_2$ tie points were estimated by considering the following two components: uncertainty of the peak positions in the filtered $\delta O_2/N_2$ curve because of the noise and resolution of the data, and possible variability of phasing between local insolation and $\delta O_2/N_2$. The former uncertainty was assessed by a Monte Carlo approach, in which the low-pass filter was applied to 1000 pseudo $\delta O_2/N_2$ datasets generated by unequally spaced re-sampling of the filtered $\delta O_2/N_2$ curve (mean interval: 512 ± 123 years) added by the following noise. For the O_2/N_2 noise, we employed standard deviations of 3.4, 1.9 and 0.4‰ for the periods of <72, 72−102, and 102−200 kyr BP, respectively, which is the residual $\delta O_2/N_2$ data after subtracting the filtered curve. The

uncertainty in the peak timing was estimated as the variability of the peak position in the 1000 low-pass filtered pseudo datasets, ranging from 99 to 551 years (1σ). We performed the same analyses using the summer solstice insolation curve at 77°S instead of the filtered $\delta O_2/N_2$ as the reference curve. The variabilities of the peak positions are 97−502 years, similar to the above results. We also applied the Monte Carlo method by simply adding noise to the original $\delta O_2/N_2$ data (instead of smoothed and re-sampled $\delta O_2/N_2$, Kawamura et al., 2007), and obtained the variabilities of 99−536 years. We used the largest of the three values for each peak for a conservative uncertainty estimate. We also found slight deviations of the average peak ages of the Monte Carlo simulation from the those in the insolation curve, within ±70 years; thus, we also included an independent error of ±50 years (1σ) for a conservative uncertainty estimate.

For the latter uncertainty (possible phase variability between insolation and $\delta O_2/N_2$), we assumed that the modern observation of variability of phasing between seasonal peaks of daily air temperature and insolation translates to the variability of phasing between $\delta O_2/N_2$ and summer solstice insolation curve for the orbital tuning (in other words, the date of the tuning target may randomly deviate from the summer solstice by the amount equivalent to the modern variability of seasonal temperature peak). The dates of peak air temperature measured by automatic weather stations at Dome Fuji between 1994 and 2001 (Takahashi et al., 2004) and 2010−2021 (Morino et al., 2021) (Fig. A2) were extracted using a general peak fitting algorithm ("Multipeak Fitting 2" package of Igor Pro®), and the variability of peak dates was found to be 2.9 days (1 σ). This roughly corresponds to 3° on the orbit, which yield the variability of the insolation peaks by ~200 years.

Assuming that the above errors are uncorrelated, the total uncertainty was estimated to be 229−588 years (1σ) by adding them in quadrature (Table 3).

2.5.3. Intervals between neighboring gas age markers (gas age intervals)

We constructed gas age intervals by matching the CH₄ record of the DF core to the records of WD CH₄ (12−29 kyr BP) and NGRIP $\delta^{18}O_{ice}$ (39−60 kyr BP) at the abrupt warming events (Tables 4 and 5). The age of the midpoints of the DO transitions for the WDC and NGRIP are taken from Buizert et al. (2015) and Svensson et al. (2020), respectively. The GICC05 chronology of the NGRIP $\delta^{18}O_{ice}$ was multiplied by 1.0063 to make it consistent with the WD2014 chronology (Buizert et al., 2015).

2.5.4. Gas depth − ice depth difference (Δdepth)

We derived Δdepth by three methods: (1) synchronization of the DF ice and gas depths with those of the WD core (0−29 kyr BP) (Fig. 4a), (2) synchronization of the DF ice and gas depths with the ice depths of the NGRIP core (33−60 kyr BP) (Fig. 4b), and (3) correlation of the abrupt CH₄ rises and corresponding Antarctic Isotope Maxima (AIM) in the DF core assuming bipolar seesaw relationship (Fig. 4c) (Parrenin et al., 2012). The obtained Δdepth are shown in Fig. 5, and numbers and uncertainties are summarized in Supplemental data.

For Method 1, the DF gas depths were matched to the WD gas depths using clear prominent variations in the CH₄ record (Fig. 2), and the WD ice depths corresponding to the gas age were transferred to the DF ice depth by interpolation between the neighboring volcanic matching points (Fujita et al., 2015; Buizert et al., 2018). For the interpolation, we used age scales (WD2014 for WDC and the tentative age scale from Step 1 for DF) rather than depth scales to consider the variations of annual layer thickness between the volcanic tie points.

For Method 2, the abrupt $\delta^{18}O_{ice}$ changes at DO warmings in the NGRIP core were matched to the corresponding DF CH₄ changes, and also to the DF ice depth by interpolation between the neighboring volcanic matching points (Supplemental data; Fujita et al., 2015; Svensson et al., 2020). For the interpolation, we used GICC05 chronology multiplied by 1.0063 (Buizert et al., 2015) for the NGRIP core, and the tentative age scale from Step 1 for the DF core.

For Method 3, we assume synchroneity between the gas depth of midpoint of an abrupt CH₄ increase and the ice depth of

Table 4
Midpoints in the DF CH₄ record for abrupt transitions, and age comparison with other records.

|	Dome Fuji (DF2021)					WAIS Divide[a] (WD2014)		Hulu[a]		NGRIP[b] (GICC05)		
	Gas depth (m)	Matching uncert. (m, 1σ)	Matching uncert. (yr, 1σ)	Gas age (yr BP)	Age uncert. (yr, 2σ)	Age (yr BP)	Age uncert. (yr, 2σ)	Age (yr BP)	Age uncert. (yr, 2σ)	Age (yr BP)	Age uncert. (yr, 2σ)	GICC05* 1.0063 (yr BP)
YD-PB	420.22	0.97	42	11550	53	**11546**	69			11619	98	
BA-YD	446.78	1.13	49	12755	74	**12769**	101			12776	135	
OD-BA	481.39	1.16	81	14560	88	**14576**	146			14643	186	
DO3	665.44	0.38	32	27725	112	**27755**	278	27922	95	27726	832	
DO4	682.20	1.49	56	28935	146	**29011**	290	29134	92	28838	898	
DO5.2	724.61	0.50	40	32503	241	32631	325	32667	236	32450	1132	**32654**
DO6	742.79	0.62	40	33832	361	33874	510	34034	337	33687	1211	**33899**
DO7	763.56	0.89	63	35592	432	35636	480	35532	299	35437	1321	**35660**
DO8	798.53	1.27	95	38330	495	38381	318	38307	155	38165	1449	**38405**
DO9	826.86	0.13	9	40297	554	40332	399	40264	241	40104	1579	**40357**
DO10	843.57	0.76	56	41622	577	41643	376	41664	310	41407	1635	**41668**
DO11	865.03	1.25	102	43521	620	43544	274	43634	144	43296	1737	**43569**
DO12	907.88	0.63	49	47026	678	47064	378	47264	153	46793	1912	**47088**
DO13	938.34	0.63	48	49432	700	49506	347	49562	251	49221	2031	**49531**
DO14	989.83	1.51	74	54362	786	54480	521			54163	2301	**54504**
DO15.2	1011.43	0.76	63	56036	825	56063	434			55737	2391	**56088**
DO16.1	1037.01	1.39	127	58255	864	58328	329			57987	2498	**58352**
DO17.1	1051.11	0.50	48	59348	906	59364	441	59364	366	59017	2556	**59389**
DO17.2	1058.63	0.74	85	59836	938	59735	333	59772	254	59385	2573	**59759**

Numbers in bold letters are used as age constraints through gas age intervals or Δdepth, for constructing DF2021.
[a] Buizert et al. (2015).
[b] Svensson et al. (2020).

Table 5
Gas age intervals from CH$_4$ matching between the DF and other cores.

Gas depth Top (m)	Gas depth Bottom (m)	Duration (yr)	1σ (yr)	Description	Chronology
420.22	446.78	1223	46	YD-PB − BA/YD	WD2014
446.78	481.39	1807	87	BA/YD − OD/BA	WD2014
481.39	665.44	13179	334	DO1 − DO3	WD2014
665.44	682.87	1256	71	DO3 − DO4	WD2014
682.87	724.61	3645	145	DO4 − DO5.2	GICC05 × 1.0063
724.61	742.79	1243	142	DO5.2 − DO6	GICC05 × 1.0063
742.79	763.56	1761	106	DO6 − DO7	GICC05 × 1.0063
763.56	798.53	2745	131	DO7 − DO8	GICC05 × 1.0063
798.53	826.86	1951	128	DO8 − DO9	GICC05 × 1.0063
826.86	843.57	1311	80	DO9 − DO10	GICC05 × 1.0063
843.57	865.03	1901	121	DO10 − DO11	GICC05 × 1.0063
865.03	907.88	3519	139	DO11 − DO12	GICC05 × 1.0063
906.86	938.34	2443	90	DO12 − DO13	GICC05 × 1.0063
938.34	989.83	4973	188	DO13 − DO14	GICC05 × 1.0063
989.83	1011.43	1584	137	DO14 − DO15	GICC05 × 1.0063
1011.43	1037.01	2264	132	DO15.2 − DO16.1	GICC05 × 1.0063
1037.01	1051.11	1036	201	DO16.1 − DO17.1	GICC05 × 1.0063
1051.11	1058.625	370	175	DO17.1 − DO17.2	GICC05 × 1.0063
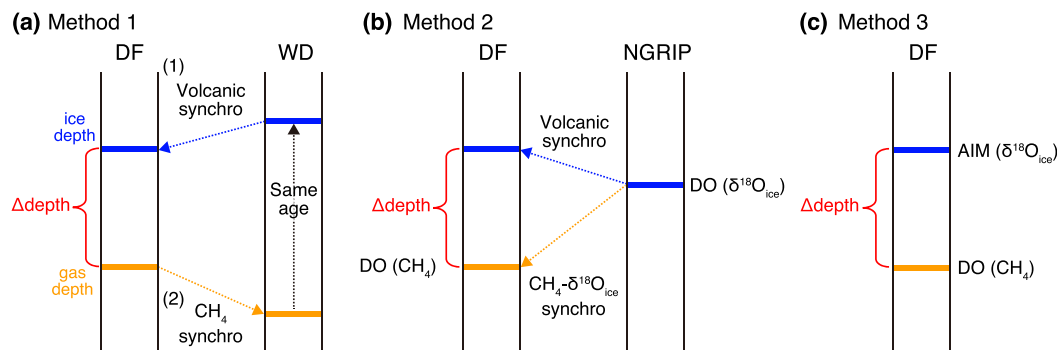
Fig. 4. Schematic of three methods for estimating Δdepth (see text for detailed explanation). DF: Dome Fuji, WD: WAIS Divide.
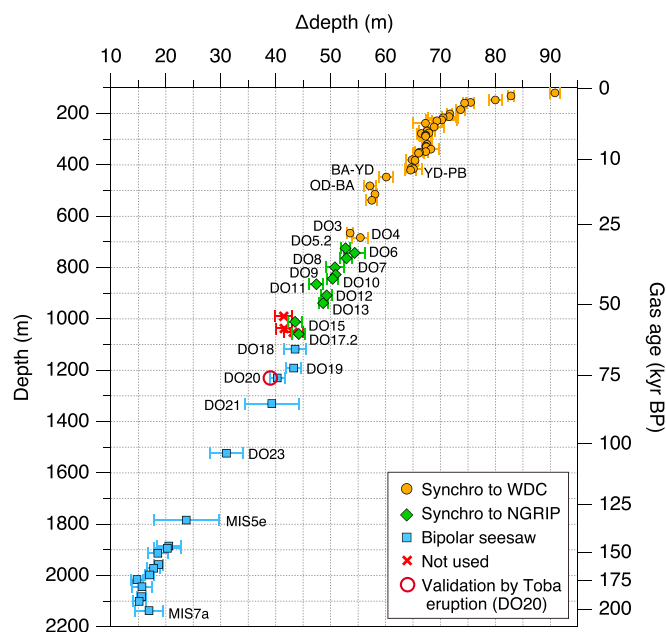
Fig. 5. Empirical Δdepth for the DF core based on the ice and gas synchronizations to the WDC and NGRIP core, or synchroneity between AIM and CH$_4$ transitions under the bipolar seesaw assumption. Δdepth for DO 14, 16.1 and 17.1 are not used for the age construction (see text). Also shown is a validation point for DO 20 by the Toba bipolar volcanic matching (Svensson et al., 2013) (see Appendix B for details).

corresponding δ^{18}O$_{ice}$ peak (highest point in the raw δ^{18}O$_{ice}$ data without smoothing, Dome Fuji Ice Core Project Members, 2017), neglecting possible slight lag (~0.1 kyr, Svensson et al., 2020).

The sources of uncertainty of Δdepth for Method 1 and 2 are the uncertainties in defining the midpoints of DO shifts (in CH$_4$ or NGRIP δ^{18}O) and in the age scales of the WD, NGRIP, and DF cores for transferring the ice depths between the cores. For Method 3, the uncertainty of Δdepth comes from those in defining the midpoints of DO shifts in the DF CH$_4$ record and the corresponding peaks (AIMs) in the DF δ^{18}O$_{ice}$ record (Table 6).

We did not use the Δdepth for some DOs whenever the CH$_4$ peak height or resolution was not enough to precisely identify the midpoints of transition (DO 14, 16.1, and 17.1), or the AIM position could not be clearly identified (DO 24). We note that if we include Δdepth for DO 14, 16.1 and 17.1, the solutions of Paleochrono show a large dip (sudden enhancement and reversal) of thinning or an extreme shallowing of LID around 1000 m (ice age: ~59 kyr BP) (Fig. 5, A3), which appears unrealistic. Such large changes in thinning over the narrow depth range is unlikely because the impurity concentrations are not particularly high or variable (Goto-Azuma et al., 2019), and the depth is relatively shallow (1/3 of the ice sheet thickness). The required LID for producing the small Δdepth is about ~90 m, which is the smallest in the studied period despite the presumably intermediate temperature in MIS 3. Although one cannot entirely rule out such a scenario (anomalously high temperature around AIM 14−16 corresponding to DO 14−16, which is missed by firn model inversion or simple δ^{18}O$_{ice}$ scaling), there is no evidence for it to reject the possible error in Δdepth. Thus, the

Table 6
Depth of AIM and CH$_4$ transitions in the DF core for deducing Δdepth, with ages in the NGRIP, Chinese cave and European cave records for comparison.

	Dome Fuji								NGRIP	Chinese cave			European cave		
	AIM(ice depth)(m)	Depthuncert.(m, 1σ)	Ice age(yr BP)	Ageuncert.(yr, 2σ)	CH$_4$ midpoint(gas depth)(m)	Depthuncert.(m, 1σ)	Gas age(yr BP)	Ageuncert.(yr, 2σ)	GICC05modelxt[a](yr BP)	Age(yr BP)	Ageuncert.(yr, 2σ)	Cave name and remarks	Age(yr BP)	Ageuncert.(yr, 2σ)	Cave name
DO18	1074.25	1.75	65074	1718	1117.81	0.88	65106	1743	64050	64500[b]	300	YX55 (after transition)			
DO19	1147.75	0.50	72467	2319	1191.06	1.25	72477	2326	72290	72200[b]	350	YX46 (within transition)			
DO20	1189.25	0.63	75979	2412	1229.56	1.25	75962	2417	76390	75500[b]	430	YX46 (within transition)	75795[f]	240	SCH 6
													75857[f]	190	BA1b
DO21	1290.25	4.38	84269	2215	1329.57	2.25	84404	2207	84710	85400[b]	600	YX46 (possibly before transition)	84671[f]	100	BA7-GAS25
										84300[c]	700	SB22 (within transition, low resolution after age marker)			
DO22					1398.80	1.13	91190	1485	89990						
DO23	1491.75	2.88	103496	1081	1522.80	0.87	103468	1118	103990				103745[f]	129	HUN14
													103640[f]	178	GAS27
													102600[g]	800	CC28
DO24	1545.75	2.13	108948	1003	1577.81	0.88	109114	1080	108230	Between 108900 ± 1100 and 110800 ± 2000[c]		SB23 (before and after transition)	108801[f]	210	HUN14
													108800[g]	1000	CC28
DO25					1619.81	1.13	114366	929	115320	113400[c]	1000	SB23 (within gradual transition)	115350[h]	500	SCH7
MIS5e	1760.05	5.63	130010	1007	1783.80	1.63	129866	1014		128950[d]	100	SB25 (within transition)	Between 129100 ±400 and 131100 ± 1200[i]		HÖL10 (before and after transition)
													Between 129600 ± 600 and 131700 ± 600[i]		SCH5 (before and after transition)
													129000[j]	1000	CC5
	1864.25	2.13	144869	1229	1884.83	0.62	144858	1283							
	1873.25	2.38	146620	1095	1893.56	0.50	146560	1166							
	1894.00	1.63	150525	549	1912.56	0.75	150355	637							
	1938.35	0.63	160710	1101	1957.06	0.50	160745	1123		161100[c]	1300	SB11 (before transition)			
										160000[c]	900	SB42 (before transition)			
	1953.26	1.00	163945	563	1971.07	0.50	163880	628		164700[c]	1700	SB11 (before transition)			
										163900[c]	1000	SB42 (before transition)			
	1980.25	0.50	169822	1191	1997.31	0.63	169817	1213		169800[e]	1000	D10 (within transition)			
	2000.13	0.72	174034	855	2014.90	0.85	173809	939							
	2027.63	1.75	180811	1036	2043.31	0.38	180808	1095		178900[c]	1400	SB11 (within transition)			
	2066.37	0.50	190434	1051	2082.00	0.72	190447	1069		190900[e]	1400	D10 (within transition)			
	2085.13	1.13	194091	959	2100.31	0.38	194058	989							
MIS7a	2119.38	1.63	200433	969	2136.35	1.88	200872	1082		199400[e]	1700				

Table 6 (continued)

Dome Fuji								NGRIP	Chinese cave			European cave		
AIM(ice depth)(m)	Depthuncert.(m, 1σ)	Ice age(yr BP)	Ageuncert.(yr, 2σ)	CH₄ midpoint(gas depth)(m)	Depthuncert.(m, 1σ)	Gas age(yr BP)	Ageuncert.(yr, 2σ)	GICC05modelxt[a](yr BP)	Age(yr BP)	Ageuncert.(yr, 2σ)	Cave name and remarks	Age(yr BP)	Ageuncert.(yr, 2σ)	Cave name
											SB11 (before transition)	Between 20100 ± 200 and 204100 ±400[k]		SPA (before and after transition)
									203900[e]	300	D8 (within transition)			

[a] Rasmussen et al. (2014).
[b] Chen et al. (2016).
[c] Wang et al. (2008).
[d] Cheng et al. (2009).
[e] Kelly (2010).
[f] Moseley et al. (2020).
[g] Boch et al. (2011).
[h] Drysdale et al. (2007).
[i] Moseley et al. (2015).
[j] Drysdale et al. (2005).
[k] Wendt et al. (2021).

anomalous Δdepth may have large errors due to the insufficient data resolution, errors in the underlying chronology (GICC05), or errors in volcanic matchings between the cores.

3. Results and discussion

3.1. New chronology (DF2021)

We obtained the new (DF2021) chronology through Step 1 - Step 9 (Section 2.1). Fig. 6 shows the constructed ice age and gas age, together with A, LID, τ, Δage, Δdepth and annual layer thickness with their uncertainties. The estimated chronological uncertainty is very small ($<\pm100$ years, 2σ) between 0 and 31 kyr BP because the chronology is densely constrained by the WD2014 chronology through the ice age intervals and Δdepth, as well as the $^{10}Be-^{14}C$ absolute age markers. The uncertainty is within ±900 years (2σ) between 31 and 60 kyr BP, where the chronology is relatively well constrained by the gas age intervals and Δdepth through the matchings with NGRIP. The largest age uncertainties of up to ±2400 years for both ice and gas are observed between 60 and 90 kyr BP where the chronology is only constrained by Δdepth from the bipolar seesaw assumption. For the period older than 90 kyr BP, the uncertainty is relatively small (~500 years) at the $\delta O_2/N_2$ tie points, and it increases to ~1300 years between the tie points.

The range of Δage in the interglacials is comprised between 2300 and 2600 years for the Holocene (the last ~12 kyr) and between 1900 and 2600 years for the last interglacial period (130−121 kyr BP). The Δage is up to ~4600 years in the glacial periods owing to a reduced accumulation rate. The values at the last and penultimate glacial maxima are similar. Compared to the previous estimate of Δage for DFO-2006 (from forward modeling using Pimienta-Barnola model), Δage of the DF2021 in the interglacial periods (Holocene and MIS5e) is ~300 years larger, while it is ~400−500 years smaller in the glacial maxima (amplitude of Δage is smaller for DF2021 Δage).

We compare the DF2021 chronology with the previous DF chronologies (Fig. 7) (DFGT-2003 by Watanabe et al. (2003b); DFO-2006 by Kawamura et al. (2007); DFGT-2006 by Parrenin et al. (2007a); N2016 by Nakano et al. (2016)). For the relatively young part (0−60 kyr BP), the previous chronologies were constrained by only one or two age control points, thus it is not surprising that they show relatively large deviations from the new chronology.

The DFGT-2003 used the orbital-scale phasing in the $\delta^{18}O_{ice}$ record for the age tie points (with error of ±6 kyr), whereas the DFGT-2006 used the $\delta O_2/N_2$ tie points with smaller error assignments ($\pm1.4-5.6$ kyr). For these chronologies, a total of five parameters in the models were inverted for the whole age range for the DF1 core (0−340 kyr BP) to minimize the overall age deviations from the tie points. Their deviations from our new chronology are within ~3 kyr, and they tend to underestimate the age for the last glacial period, and overestimate it in the penultimate glacial period.

On the other hand, DFO-2006 applied posteriori age correction to DFGT-2003 to strictly pass through the $\delta O_2/N_2$ tie points (older than ~80 kyr BP), and the N2016 chronology employed a sequential Bayesian approach to locally adjust the accumulation rate and thinning function to reproduce the $\delta O_2/N_2$ tie points within error. Thus, they are similar to each other for period older than ~80 kyr BP, and their errors reflect those of the $\delta O_2/N_2$ tie points, which are placed roughly every 11 kyr. The possibility of large error of the DFO-2006 chronology was pointed out by Fujita et al. (2015) that the $\delta O_2/N_2$ age marker at 94.2 kyr BP was older by ~3 kyr than the U−Th chronology of Chinese speleothem (Barker et al., 2011). Error of DFO-2006 for this age was also suggested from a large step-like change in the annual layer thickness at 92 kyr BP, calculated directly from the DFO-2006 chronology (1376 m, Fig. 6), while there

is no such step in the $\delta^{18}O_{ice}$ profile. The DF2021 chronology (with improved $\delta O_2/N_2$ dataset) gives the age of 94.2, 116.7 and 126.4 kyr BP to the old $\delta O_2/N_2$ age markers, which are younger than DFO-2006 by 1.6, 1.0 and 1.3 kyr, respectively. Between 145 and 190 kyr BP, the old $\delta O_2/N_2$ tie points are shifted by about 1 kyr toward the older direction.

3.2. Glaciological parameters and sensitivity test

The average accumulation rate over the Holocene is estimated to be 2.94 cm-of-ice yr^{-1} with the maximum of 3.15 cm-of-ice yr^{-1} in the early part, and 3.87 cm-of-ice yr^{-1} for the peak of the last interglacial period (128.3−131.5 kyr BP, Fig. 6d). The accumulation rate is 1.85 cm-of-ice yr^{-1} on average in the last glacial period

(19−111 kyr BP), with the minima in the LGM and MIS 4. The values in MIS 6 are similar to the LGM value. In general, the accumulation rates from the initial and intermediate steps in this study (Step 1 and Step 7) as well as previous estimates (Parrenin et al., 2007a; Dome Fuji Ice Core Project Members, 2017) agree with the final result of this study (after Step 9) within the estimated uncertainty. The difference between the final accumulation rate (from Paleo-chrono probabilistic model) and that after Step 7 (from DynaDens firn model) is mostly less than 10%. The close agreement on past accumulation rates is owing to the high-resolution $\delta^{15}N$ and Δage data available for the DF core, which together strongly constrain past A.

The thinning function in the final result agrees within 10% with the initial scenario from the ice flow model of Parrenin et al.
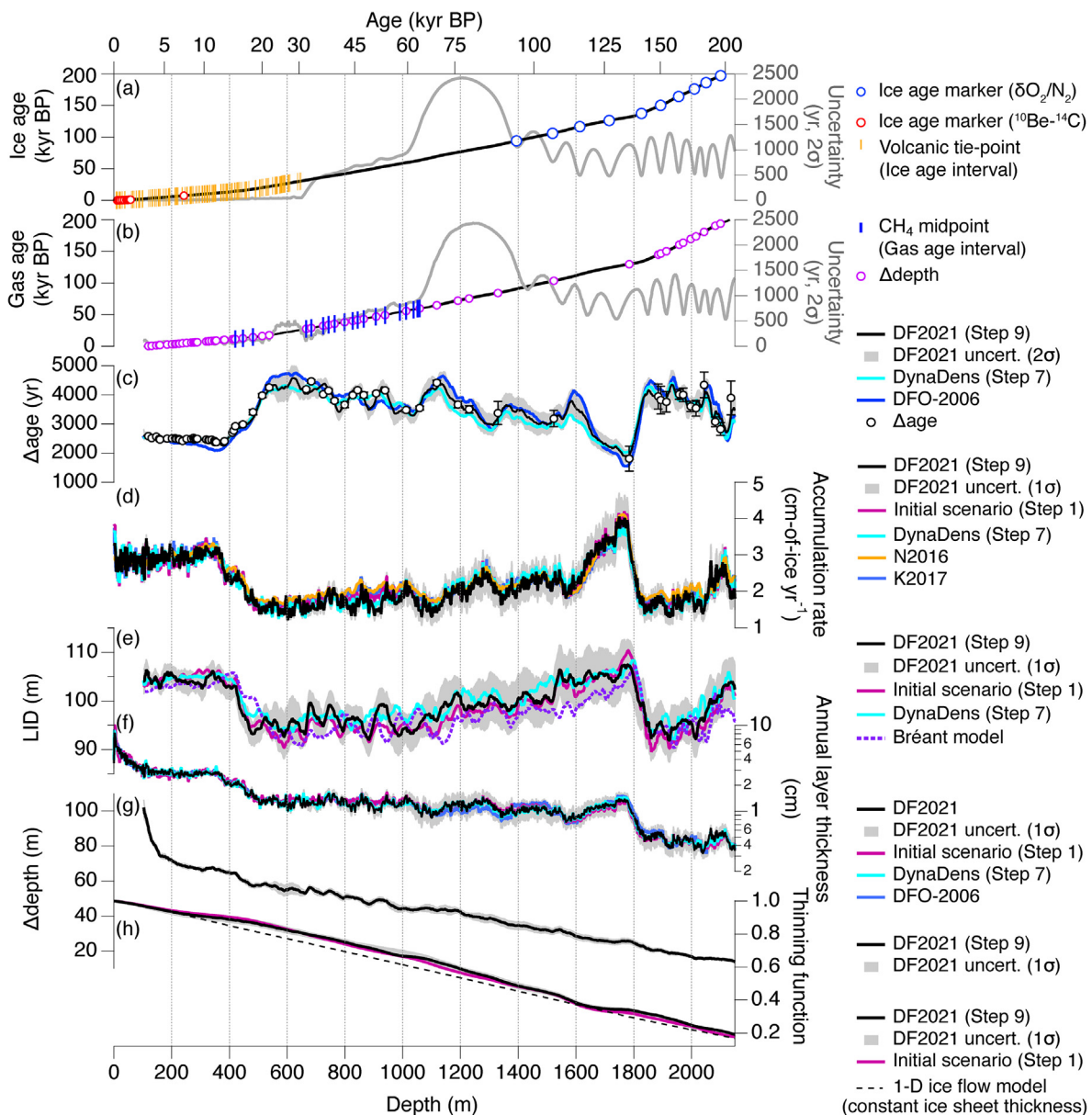
Fig. 6. The DF2021 chronology and associated glaciological parameters. (a) Ice age scale with 2σ uncertainty, and ice age constraints. (b) Gas age scale with 2σ uncertainty, and gas age and Δdepth constraints. (c) Δage with 2σ uncertainty, intermediate Δage from the firn model, and previous Δage in DFO-2006 (Kawamura et al., 2007). (d) Accumulation rate with 1σ uncertainty, initial scenario, intermediate scenarios from firn models, and previous studies (Nakano et al., 2016; Dome Fuji Ice Core Project Members, 2017). (e) Same as (d) but for LID. (f) Same as (d) but for annual layer thickness. (g) Δdepth with 1σ uncertainty. (h) Thinning function with 1σ uncertainty, initial scenario, and model result with constant ice thickness.

(2007a), which incorporate glacial-interglacial variations in ice sheet thickness (thinner in glacial periods) (Fig. 6h). Even if we start from a simpler initial scenario with a constant ice sheet thickness (fixed to present-day, Run 3 in Table 7), the final thinning function significantly deviates from the initial scenario below ~300 m to become in agreement with the standard result (Fig. 8f and i, magenta). This demonstrates the performance of Paleochrono model, which can reasonably correct the glaciological parameters with the chronological constraints used in this study.

The average LID is ~104 m in the Holocene and ~95 m in the LGM (19−28 kyr BP) (Fig. 6e). Overall, the LID from the final result (Step 9) agrees with those based on both the δ^{15}N data (Step 1) and the DynaDens firn model (Step 7, constrained by δ^{15}N and Δage data) within the estimated uncertainty of the final result. For example, the difference between the LID of Step 9 and that of Step 7 is mostly within 5%.

To examine whether the chronology after Step 9 (Paleochrono) is sensitive to the prior of LID, A and τ used in the intermediate steps, we tested the method with another firn densification model (Bréant model, Bréant et al., 2017), accumulation histories and thinning function. The Bréant model employs reduced temperature sensitivity at low temperatures and introduced the hypothetical influence of impurities in softening the firn, which enhanced densification rates in dusty glacial periods. The model required T, A and Ca^{2+} concentration as input data. For the test, we adjusted the amplitude of ΔT_{site} (Uemura et al., 2018) for obtaining T that matched the glacial-interglacial difference in δ^{15}N and Δage data, while we fixed A and Ca^{2+} scenarios. A was derived from the posterior after Step 9 (i.e., the final result from Paleochrono). The Ca^{2+} record was taken from Goto-Azuma et al. (2019) (Fig. A4c), with replacement of relatively poor-quality data from the latter part of the last termination to early Holocene by linearly interpolating between four data points at 14.5, 12.8, 11.8 and 8.6 kyr BP to reject unnaturally high scatter. The T thus tuned shows the glacial-interglacial difference of about 15 °C (Fig. A4b), which would give different temperature profile in the firn (and thus δ^{15}N$_{therm}$) from the those with the DynaDens model (Fig. A4g-i).

The LID from the Bréant model and DynaDens model (Step 7) agree with each other and reproduce thinner firn in the glacial period (Fig. 6e, A4f). Note that the temperature histories are largely different for the different densification models, but the resulting LID histories are similar, albeit with some differences. For example, the onset of LID deepening (reduction) for Termination I (after the

last interglacial period) is earlier in the Bréant model result. The differences are due to the different timings of T and A changes (Fig. A4a, A4b), which in turn is due to the difference in how the models are run; while the Bréant model uses T from linear scaling of the original ΔT_{site} (Uemura et al., 2018) and allows some misfits with the δ^{15}N data, the DynaDens model locally inverts T and A (i.e., modify the shape of original ΔT_{site}) to closely follow the δ^{15}N data. The amplitude of δ^{15}N$_{therm}$ of the DynaDens model is generally smaller than that of the Bréant model due to smaller surface temperature variations.

To examine the sensitivity of the resulting chronology to the initial conditions, we run Paleochrono with different combinations of A, LID and τ as shown in Table 7. In all cases, the differences in age between the alternative results and the standard results are much smaller than the estimated uncertainties (Fig. 8a and b), with the maximum differences of 373 and 349 yr for ice and gas age, respectively, at around 70 kyr BP where the age constraints are weak (see above). The ice age is most sensitive to prior A (Run 2), while the gas age is sensitive to both prior A and LID (Run 2, 6). The prior LID appears to affect gas age through its effect on Δage (note the similarity between gas age and Δage deviations). The change of prior τ has small impact on the final chronology (less than 120 yr) (Run 3).

The difference of δ^{15}N$_{therm}$ (Run 1 and 5), which is subtracted from the δ^{15}N data to deduce prior LID (Fig. A4f), between the Bréant and Dynadens models does not affect the chronology by more than 50 years on average with the maximum difference of ~200 years, because the δ^{15}N signal is dominated by δ^{15}N$_{grav}$ (Fig. 8e). The use of modeled LID (Run 4 and Run 6) also does not significantly affect the chronology. We prefer to use the prior LID from the δ^{15}N data corrected with the modeled δ^{15}N$_{therm}$, because the δ^{15}N signal is dominated by LID and it is difficult to perfectly reproduce δ^{15}N data by the firn models. In any case, the differences in gas age and Δage when using different prior LIDs are less than ~400 years (Fig. 8b and c). Around the onset of the Termination I and II (~19 and ~140 kyr BP), which are important for paleoclimatic discussion (e.g., lead/lag of temperature and CO_2), Δage from all runs agree with each other fairly well (within 200 years).

3.3. Comparison with other chronologies

We compare our new DF2021 chronology with the following chronologies: (1) WD2014 and GICC05 as well as U−Th chronology
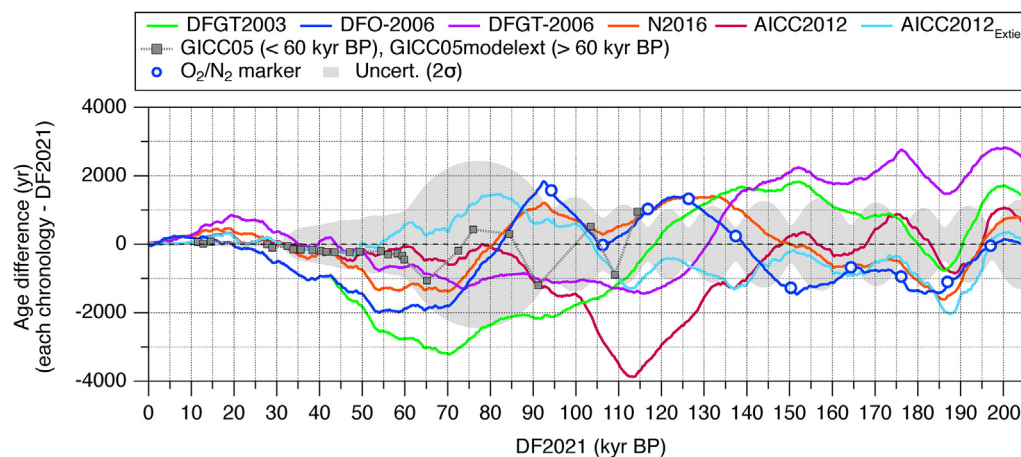

Fig. 7. Age difference between DF2021 and previous DF chronologies as well as AICC2012, AICC2012$_{Extier}$ and GICC05. DFGT-2003: Watanabe et al. (2003b), DF0-2006: Kawamura et al. (2007), DFGT-2006: Parrenin et al. (2007a), N2016: Nakano et al. (2016), AICC2012: Veres et al. (2013); Bazin et al. (2013), AICC2012$_{Extier}$: Extier et al. (2018), GICC05: Vinther et al. (2006); Andersen et al. (2006); Rasmussen et al. (2006); Svensson et al. (2006); Svensson et al. (2008), and GICC05modelext Wolff et al. (2010); Johnsen et al. (2001).

Table 7
Combination of *A*, LID and τ for the sensitivity test.

Run No.	Run name	*A*	LID	τ
1	Step 9_STD	DynaDens (Step 7)	$\Delta^{15}N$ data corrected with DynaDens$\delta^{15}N_{therm}$ (Step 8)	After Step 2_STD
2	Step 9_*A*	1-D ice flow model (Step 1)	$\delta^{15}N$ data corrected with DynaDens$\delta^{15}N_{therm}$ (Step 8)	After Step 2_STD
3	Step 9_τ	DynaDens (Step 7)	$\delta^{15}N$ data corrected with DynaDens$\delta^{15}N_{therm}$ (Step 8)	1-D ice flow model (constant ice sheet thickness)
4	Step 9_LID (DynaDens)	After Step 9_STD	DynaDens (Step 7)	After Step 2_STD
5	Step 9_LID (Bréant$^{15}N_{therm}$)	After Step 9_STD	$\delta^{15}N$ data corrected with Bréant$\delta^{15}N_{therm}$	After Step 2_STD
6	Step 9_LID (Bréant)	After Step 9_STD	Bréant model	After Step 2_STD
7	Step 2_STD	1-D ice flow model (Step 1)	$\delta^{15}N$ data corrected with constant $\delta^{15}N_{therm}$ (Step 1)	1-D ice flow model (Step 1)

of Chinese speleothem (Hulu) for the last 60 kyr, (2) AICC2012 and GICC05modelext as well as U−Th chronology of Chinese and European (Switzerland and Austria) speleothems for 60−130 kyr BP, and (3) U−Th chronology of Chinese speleothem (Sanbao and Dongge) for 130−200 kyr BP.

3.3.1. Last 60 kyr

First, we compare DF2021 with the layer-counted WD2014 and GICC05 chronologies that were used to constrain DF2021 through the ice age and gas age intervals. Fig. 9 shows the age differences between DF2021 and WD2014 or GICC05 chronologies.

For the last 30 kyr, the comparisons between DF2021 and WD2014 at the volcanic and CH_4 match points (this study) show that the DF2021 ice and gas ages agree with those of WD2014 within 20 and 80 years, respectively, with DF2021 being slightly younger than WD2014 (by 10 yr on average for 93 points and 20 yr on average for 12 points for ice age and gas age, respectively) between 10 and 30 kyr BP. We note that the DF2021 - WD2014 gas age difference is 56 yr at 23.9 kyr BP where the estimated gas age uncertainty is relatively large (~400 yr, 2σ), suggesting that the actual error of DF2021 is smaller than the statistical error estimate around this age.

Between 30 and 60 kyr BP, the comparisons between DF2021 and GICC05 × 1.0063 can be made either by the CH_4 (DF gas) − $\delta^{18}O_{ice}$ (NGRIP ice) matching at abrupt changes (this study) and the bipolar volcanic matching (DF ice − WDC ice − NGRIP ice) (Svensson et al., 2020 and this study). The difference between DF2021 and GICC05 × 1.0063 is smaller than 160 and 150 years for the DF ice and gas age, respectively. The differences between DF2021 (gas) and WD2014 (gas) at the match points are similar to those between DF2021 (gas) and GICC05× 1.0063 (ice), as expected from the fact that the construction of WD2014 (gas) incorporated the matching to GICC05× 1.0063 (ice) (Buizert et al., 2015). On the other hand, a relatively large difference of up to 502 years is observed between DF2021 (ice) and WD2014 (ice) for the 50−55 kyr BP period, although it is within the 2σ uncertainty of WD2014. This interval corresponds to the long-duration DO interstadial 14, during which there were no interpolar CH_4 tie points to anchor the WD2014 chronology (Buizert et al., 2015); the deviation may thus reflect an interpolation artifact in WD2014. For this period, the age difference is small around the CH_4 tie points (at ~49 and 54 kyr BP) and it rapidly increases towards the largest difference at ~53 kyr BP. Considering that the difference between WD2014 and GICC05 × 1.0063 is also largest in this range, and that the difference between DF2021 and GICC05× 1.0063 is relatively small, the relatively large WD2014 - DF2021 ice age difference might suggest somewhat large error in the WDC Δage close to the bedrock.

The gas age scale of an ice core (CH_4) can be compared with U−Th age scales of speleothems ($\delta^{18}O$) for the abrupt climate changes (e.g., Buizert et al., 2015). For 13 points of the DF − Hulu comparison between 27 and 60 kyr BP (Table 4, Fig. 9), DF2021 (gas) agrees with the Hulu chronology within 239 years, which are

mostly within the estimated 2σ uncertainty of DF2021. The differences are small also for the period older than ~35 kyr BP where the 2σ uncertainty becomes larger than ~400 yr (up to ~900 yr around 60 kyr BP).

3.3.2. 60−130 kyr BP

Between 60 and 130 kyr BP, we compared DF2021 with AICC2012 and GICC05modelext (GICC05 extended by the model-based ss09sea age scale with −704 yr offset, (Wolff et al., 2010; Johnsen et al., 2001), as well as the updated AICC2012 chronology with revised age markers by matching rapid changes in $\delta^{18}O_{atm}$ of the EDC core with those in $\delta^{18}O$ of Chinese speleothems for the period older than 100 kyr BP (hereafter AICC2012$_{Extier}$, Extier et al., 2018). We also directly compared DF2021 with U−Th chronologies of Chinese and European (northern rim of the Alps, hereafter NALPS and Italian) speleothems (Wang et al., 2001, 2008; Cheng et al., 2009; Kelly et al., 2006; Kelly, 2010; Chen et al., 2016; Boch et al., 2011; Moseley et al., 2015, 2020; Drysdale et al., 2005, 2007) (Fig. 10) using abrupt CH_4 shifts and corresponding calcite- $\delta^{18}O$ transitions in the speleothem records. This period contains 9 points for precise age comparisons (onsets of DO 18−25 and the end of Termination II). We do not compare the timing of the rapid changes in $\delta^{18}O_{atm}$ of the DF core with those in $\delta^{18}O$ of Chinese speleothems as Extier et al. (2018) conducted.

For DO 18, the midpoint of DF CH_4 transition on DF2021 is 65.1 ± 1.7 kyr BP, which agrees with WD2014, AICC2012, and GICC05modelext within the estimated uncertainties. For the older period, according to the volcanic matching between the DF and EDC cores by Fujita et al. (2015), the DF2021 chronology agrees with AICC2012 within 2 kyr except for large discrepancy between ~103 and 128 kyr BP of up to 3.9 kyr at ~110 kyr BP (Fig. 7), whereas it agrees well with AICC2012$_{Extier}$. The DF2021 chronology agrees with GICC05modelext within ~1 kyr at all DO transitions in this range (Figs. 7 and 10).

The differences between DF2021 and U−Th ages are generally smaller than 1 kyr and within the 2σ uncertainty of DF2021. The good agreement between the DF2021 and the speleothem chronologies are remarkable for the independent age scales in this range. Below, we discuss the comparisons in detail, using the DO transitions in the Chinese speleothem records if they can be clearly identified with U−Th-dated points in or close to the transition, as well as all DO ages in the NALPS speleothem records as given in Boch et al. (2011) and Moseley et al. (2020).

For DO 18, 19, 20 and 21, the available U−Th ages of Chinese or European speleothem records all agree with DF2021 within uncertainties (Table 6), although some of the DO transitions are gradual or ambiguous in the speleothem records (for example, gradual DO 21 transition in the SB22 and SB25). The lack of age control on the DO 22 transition in the speleothem records make it difficult to compare the chronologies at this transition. We may instead be able to compare a possible cooling event after DO 22 (88.8 ± 0.9 kyr BP in the DF CH4 record) with the NALPS record
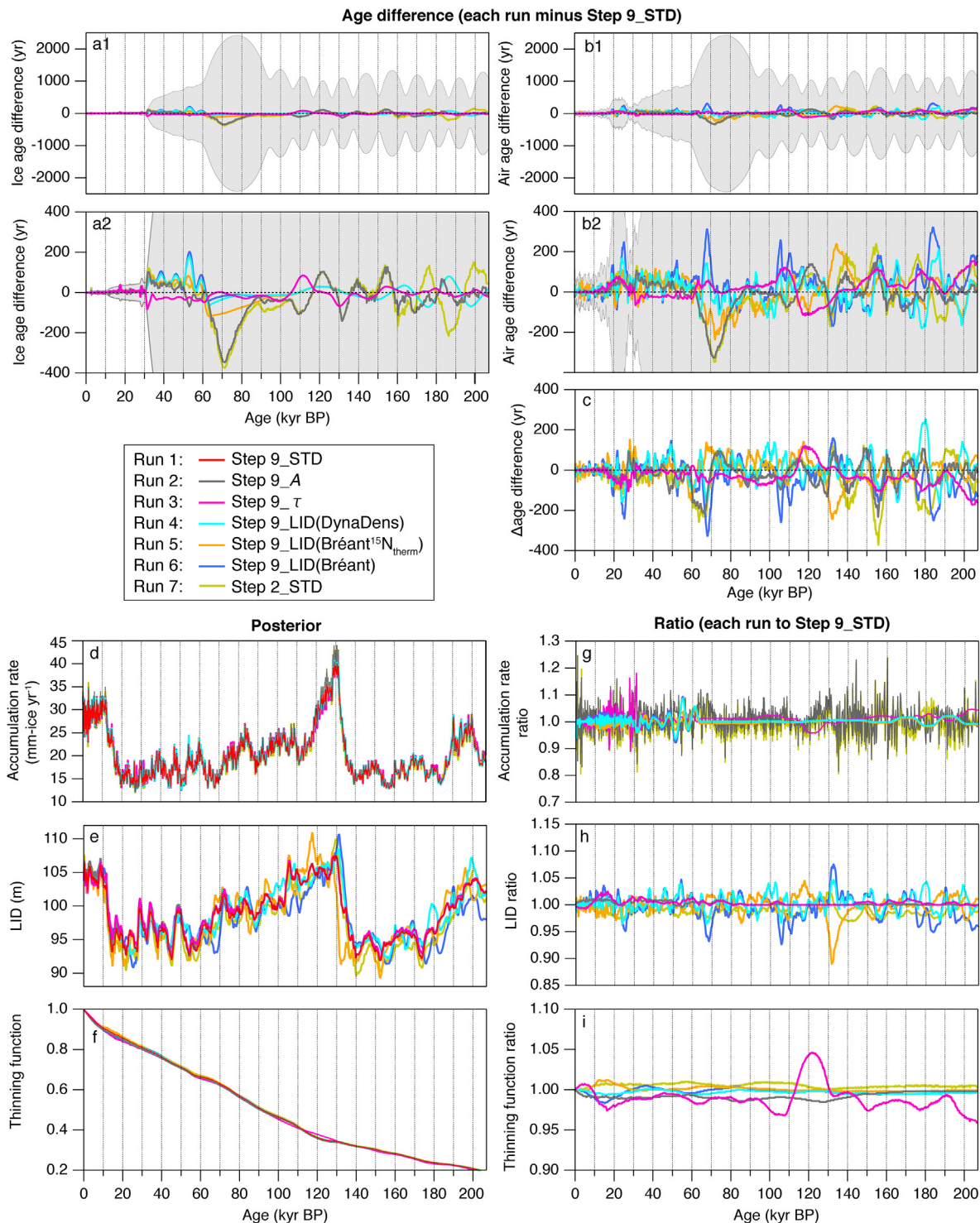
Fig. 8. Results of the sensitivity test. (a1) Ice age difference from each run minus standard result (Run 1), with DF2021 ice age uncertainty (2 σ). (a2) Enlarged view of (a1). (b1) Same as (a1) but for gas age. (b2) Same as (a2) but for gas age. (c) Same as (a2) but for Δage. (d–f) Posteriors for accumulation rate, LID and thinning function, respectively, from Run 1 − Run 7. (g–i) Ratios of each run to Run 1 for accumulation rate, LID and thinning function, respectively.

(88.7 ± 0.2 kyr BP). For DO 23, the DF CH$_4$ transition agrees with the U−Th ages of NALPS (Table 6) as well as an Italian speleothem (Drysdale et al., 2007). We find it difficult to compare this transition with the Chinese records because of their different signal shapes (Fig. 10); the NGRIP δ^{18}O$_{ice}$, DF CH$_4$ and NALPS δ^{18}O records commonly show a stadial period between DO 23 and 24 for about 1500 years, which is extremely short in the Chinese δ^{18}O records

possibly suggesting local environmental signals. For DO 24 and 25, the ages of DF CH$_4$ transitions agree with those of NALPS, Chinese and Italian speleothem records within the 2σ uncertainty of DF2021. We note that not all Chinese speleothem records show the DO 25 transition. The abrupt climate change at the end of Termination II is dated at 128.95 ± 0.10 kyr BP in the Chinese speleothem record (SB25, Cheng et al., 2009). The NALPS records probably do
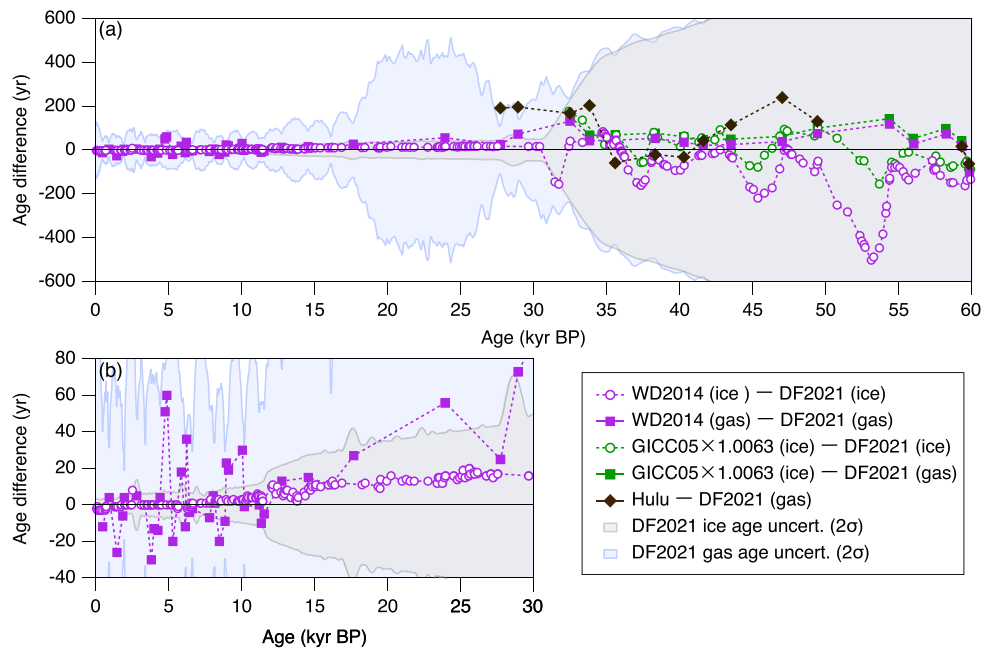
Fig. 9. Age difference between DF2021 and other chronologies for the last 60 kyr.

not cover the early part of Termination II, but the abrupt transition at the end of Termination is clearly visible with the age between 129.1 ± 0.4 and 131.1 ± 1.2 kyr BP (HÖL10), and between 129.6 ± 0.6 and 131.7 ± 0.6 kyr BP (SCH5) (Moseley et al., 2015). The end of Termination II is dated at 129 ± 1 kyr BP in an Italian speleothem record (Fig. 10, Drysdale et al., 2005). The abrupt CH_4 rise on DF2021 is seen at 129.8 ± 1.0 kyr BP, consistent with the speleothem ages.

For the above comparison points (n = 9), the abrupt CH_4 changes on the DF2021 chronology are older by +0.1 ± 0.3 kyr on average than the corresponding events in the U−Th-dated Chinese or European stalagmites. Considering the uncertainty of DF2021, the differences are insignificant. The excellent agreement of DF2021 with the U−Th chronology suggests high accuracy of our chronology, and support the assumption of zero phasing between the past local summer solstice insolation and $\delta O_2/N_2$ fractionation for constructing the age markers. The previously reported discrepancies between the $\delta O_2/N_2$ records of different deep ice cores with short-term scatters (Bazin et al., 2016) may be a result of poor quality of the previous datasets (mainly due to gas loss during sample storage), at least for the DF core.

3.3.3. 130−207 kyr BP

We compared DF2021 with AICC2012 and AICC2012$_{Extier}$ as well as U−Th chronologies of Chinese and Austrian speleothems (Cheng et al., 2009, 2016; Kelly et al., 2006; Kelly, 2010; Wendt et al., 2021) (Fig. 10). The DF2021 chronology agrees with the AICC2012 and AICC2012$_{Extier}$ chronologies within 2 kyr (<1 kyr before 140 kyr BP) (Fig. 7).

As in the last glacial period, we now compare the chronologies for MIS 6 using the abrupt CH_4 shifts and corresponding calcite-$\delta^{18}O$ transitions in the speleothem records, if a U−Th dating point is located at or close to the events. We identified 16 events of CH_4 increase in the DF data for the potential age comparison between 130 and 207 kyr BP (vertical lines in Fig. 10). However, there is generally lower degree of similarity between the variations in CH_4 and $\delta^{18}O$ (speleothem) in the penultimate glacial period than in the last glacial period. We also note that the speleothem U−Th ages or the shapes of $\delta^{18}O$ curves disagree with each other for the same

events (for example, around the large peak at about 195−200 kyr BP). Possible reasons for the dissimilarity include local climatic influence in the speleothem $\delta^{18}O$ record (e.g., Moseley et al., 2015), overall low resolution of the records (both CH_4 and $\delta^{18}O$), two long periods of muted variabilities where no common events could be identified (around 155 and 185 kyr BP), generally small amplitudes of CH_4 peaks, and disagreements of timing of some abrupt shifts between the stalagmite records in relation to generally larger uncertainty of U−Th dating (±1.3 kyr on average for the Chinese speleothems). Thus, for some of the events, it is difficult to find the counterparts of the DF CH_4 events in the speleothem records (dashed vertical lines in Fig. 10). We could finally identify 8 events with 11 U−Th dates for the age comparisons, for which the DF2021 chronology is older by +0.1 ± 1.3 kyr (n = 12) on average than the U−Th chronology. If we remove one event (three U−Th ages) at ~200 kyr BP from the comparison, where U−Th ages disagree by more than 4 kyr to each other, the mean difference becomes −0.2 ± 0.8 kyr (n = 9). The agreement is excellent considering their uncertainties.

3.4. Phase variability between $\delta^{18}O_{atm}$ and 65°N summer solstice insolation

The DF2021 chronology may provide reliable durations of climatic events, e.g., the last interglacial period (MIS 5e), and the timing of the last glacial inception (MIS 5e − 5d transition) and other transitions in MIS 5 substages, where the previous ice core chronologies have shown relatively large discrepancies. On DF2021, the initial Antarctic cooling (lowering of $\delta^{18}O_{ice}$ for MIS 5e − 5d) and subsequent transitions between the MIS 5 substages are broadly in phase with 65°N summer solstice insolation (and the precession parameter) (middle panel of Fig. 10). As shown in the previous section, the AICC2012 chronology from 103 to 126 kyr BP (roughly from the latter part of the last interglacial period to the last glacial inception) is younger by ~2−4 kyr than DF2021 (maximum deviation in MIS 5d at ~110 kyr BP), and the difference becomes insignificant (<~1 kyr) around ~90 kyr BP. Thus, our new chronology supports the suggestion by Fujita et al. (2015), Extier et al.
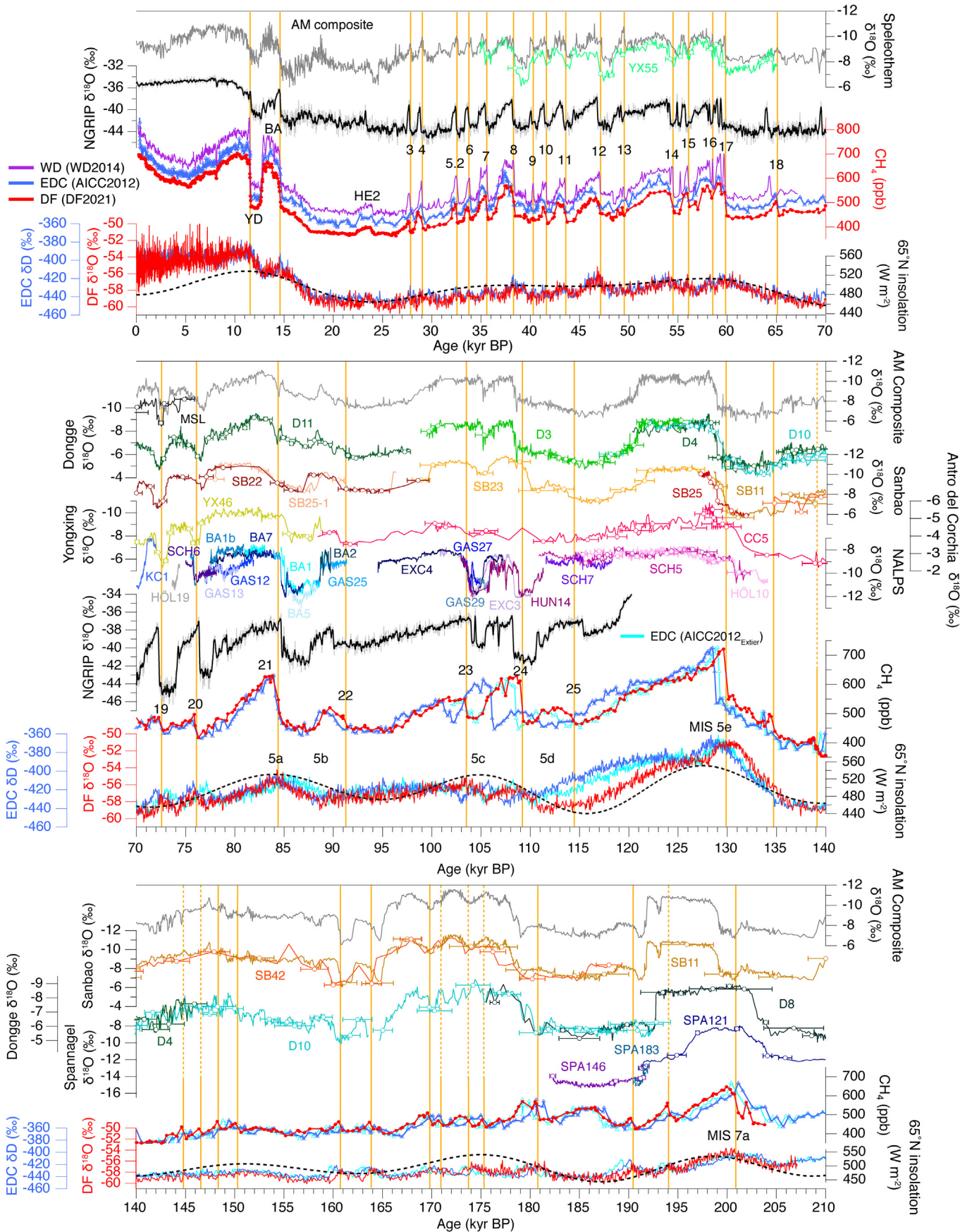
(2018) or Moseley et al. (2020) that AICC2012 is likely too young around 110 kyr BP based on the comparison between the AICC2012 and U−Th speleothem chronologies.

We consider possible causes for the large changes of age discrepancy within the relatively short intervals around MIS 5d. If the prior of accumulation rate is significantly overestimated around MIS 5d, which was converted from water isotopic record (Parrenin et al., 2007a; Bazin et al., 2013), it might be reflected in the posterior and cause unrealistically thick annual layers and longer duration from MIS 5e to 5d (Fujita et al., 2015; Parrenin et al., 2016). To evaluate this possibility, we calculated the ratio of the posterior accumulation rate for the EDC core (from AICC2012) to that for the DF core (from DF2021), and compared it with the ratio based on detailed age synchronization between the cores (Parrenin et al., 2016) (Fig. A5). From the last interglacial to the present, the EDC/ DF accumulation ratio from the posteriors agrees well with that from the synchronization except for the period from ~115 to ~80 kyr BP where the former ratio is significantly larger for prolonged times. The discrepancy in this period is also seen in the isotope-based accumulation (Parrenin et al., 2016), suggesting that the posterior accumulation of the EDC core is indeed overestimated.

However, because the prior accumulation rate, thinning and LID are modified along depth to follow the age markers within uncertainties, the errors in the priors are expected to be reduced in the posteriors if the age markers are accurate. On the contrary, the posterior accumulation rate for EDC (Veres et al., 2013; Bazin et al., 2013) is larger than the prior (isotope-based) accumulation rate (Parrenin et al., 2007a) around 100−105 kyr BP (Fig. A3). In addition, while the prior thinning function monotonically decrease with depth, the posterior shows a small reversal for 1355−1383 m (around 100 kyr BP, about the same range as the overestimated accumulation) (Fig. A5). From the fact that both the posteriors of accumulation rate and thinning function enhanced the thicker annual layers and led to younger MIS 5d in AICC2012, we turn to the errors of age markers as the dominant cause of the age error (Veres et al., 2013; Extier et al., 2018).

The age markers for 100−130 kyr BP used in AICC2012 are one $\delta O_2/N_2$ marker (121.8 kyr BP, ice age) and three $\delta^{18}O_{atm}$ markers (100.4, 110.6 and 121.9 kyr BP, gas age) in the Vostok core, and one air content marker (100.95 kyr BP, ice age) in the EDC core. The Vostok $\delta^{18}O_{atm}$ data were smoothed and matched to 65°N summer solstice insolation at every midpoints between peaks and troughs with the phase lag of 5.9 kyr (Suwa and Bender, 2008), with the assigned uncertainty of ±6 kyr (about a quarter of a precession cycle). Extier et al. (2018) investigated phase variability of $\delta^{18}O_{atm}$ on AICC2012 and suggested that the large lag (5 or 6 kyr) of $\delta^{18}O_{atm}$ behind 65°N summer insolation is mainly due to Heinrich Events (HE) particularly during deglaciations, and that the alignment of $\delta^{18}O_{atm}$ to insolation with a constant 5-kyr lag could produce large errors. Instead, they proposed to use U−Th-dated $\delta^{18}O$ records of Chinese speleothems as the tuning target, and updated the AICC2012 chronology (AICC2012_Extier). As shown in section 3.3.2, AICC2012_Extier agrees with DF2021 around 110 kyr BP. We note that AICC2012_Extier is consistently younger than DF2021 for most of the period before ~105 kyr BP where it is revised by the new age markers (Fig. 7), possibly suggesting some minor bias in the alignment between the ice-core $\delta^{18}O_{atm}$ and speleothem $\delta^{18}O$

records.

Here, we analyze the phase variability between $\delta^{18}O_{atm}$ of the DF core (Kawamura et al., 2007) on DF2021 and 65°N summer solstice insolation. Our chronology is suitable for this analysis because it has the advantage over the previous DF chronologies that used conventional firn densification modeling to estimate the gas age. For smoothing the $\delta^{18}O_{atm}$ record, we used the same low-pass filter as used for the $\delta O_2/N_2$ data (cut-off from 16.7 to 10.0 kyr; Kawamura et al., 2007, see section 2.5.2), and age of the midpoints in the insolation curve were compared with the corresponding midpoints in the filtered $\delta^{18}O_{atm}$ curve (Table 8, Fig. 11). Because the precessional amplitude is too small in the $\delta^{18}O_{atm}$ record around 41.8 and 157.3 kyr BP to precisely determine the midpoints, we omit these points from the analysis. The result shows that the DF $\delta^{18}O_{atm}$ signal lags behind 65°N summer solstice insolation by 6.4 kyr for the most recent midpoint, but the average lag is only 4.1 ± 1.4 kyr (one standard deviation) over the last 207 kyr. In particular, the lags for the insolation midpoints at 100.4, 110.6 and 121.9 kyr BP are only 2.7, 1.4 and 2.4 kyr, respectively, which are the only cases to show consecutive deviations of more than 3 kyr from the assumed constant lag for AICC2012. We also find that the large lags of $\delta^{18}O_{atm}$ behind 65°N summer insolation are not only seen at HE during deglaciations as suggested by Extier et al. (2018), but also during the glacial periods for the insolation midpoints at 30.0, 65.5 and 145.4 kyr BP. On the other hand, the lag for HE11 during Termination II (133.5 kyr BP in insolation midpoint) is a modest value of 4.1 kyr. The small number of cases preclude robust discussion, but we note that HE11 was not a typical HE with massive ice discharge through Hudson Straight as documented by the lack of detrital carbonate content in a marine sediment core, with possible implication that the Laurentide ice sheet was smaller and thinner during MIS6 (Obrochta et al., 2014). Thus, the area of freshwater input in the northern North Atlantic may have been different from that for the HEs during the last glacial and deglacial periods, possibly leading to weaker response of climate and hydrological cycle during HE11. The large lag for 65.5 kyr BP may be caused by the HE6 that may have enriched terrestrial precipitation $\delta^{18}O$ for prolonged time (Extier et al., 2018), but the lags for 30.0 and 145.4 kyr BP should not be directly caused by HE because they are in the increasing phase (towards more glacial-like value) of $\delta^{18}O_{atm}$. It may be possible that the HE1, 2, and 11 shifted the timings of the $\delta^{18}O_{atm}$ maxima (around the last and penultimate glacial maxima) towards the younger ages and thus also shifted the prior midpoints. Thus, the phasing between $\delta^{18}O_{atm}$ and 65°N summer insolation does not appear to be simply related to HE, and it is beyond the scope of this study to fully investigate the determining factors of the lag (presumably requiring the precise knowledge of timing of changes in ice sheet volume and precipitation $\delta^{18}O$ in different latitudes).
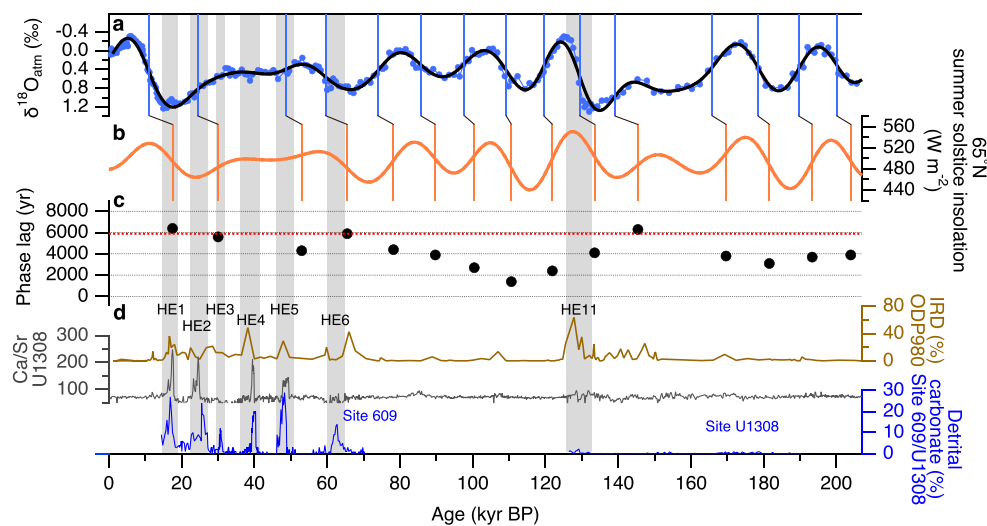
4. Conclusion

We constructed a new chronology (DF2021) for the Dome Fuji ice core for the last 207 kyr, fully utilizing the recent and significant progress in chronological constraints and dating tools, as summarized below. (1) It has become possible to synchronize the DF ice and gas age for the last 60 kyr to those of layer-counted ice cores and tree

Fig. 10. Comparison of chronologies between DF2021, AICC2012, AICC2012_Extier, GICC05 and speleothem U−Th ages. Vertical lines indicate the timing of CH_4 transitions on the DF2021 chronology. U−Th ages are indicated by markers with 2σ error bars except for NALPS records, which have numerous age measurements (not shown for visibility). NGRIP record is shown on the original GICC05 chronology (not multiplied by 1.0063). The CH_4 records of the WD and EDC cores for 0−70 kyr BP are plotted with offsets of +90 and + 45 ppb, respectively, for clarity. The plotted records and references are as follows. DF CH_4: This study; Buizert et al. (2021), DF $\delta^{18}O_{ice}$: Dome Fuji Ice Core Project Members (2017), EDC CH_4: Loulergue et al. (2008); Shin et al. (2020), EDC δD: Jouzel et al. (2007), WD CH_4: Rhodes et al. (2015), NGRIP $\delta^{18}O_{ice}$: NGRIP members (2004), Asian monsoon (AM) composite: Cheng et al. (2016), Hulu cave: Wang et al. (2001), Dongge cave: Kelly et al. (2006); Kelly (2010), Sanbao cave: Wang et al. (2008); Cheng et al. (2009), Yongxing cave: Chen et al. (2016), NALPS: Boch et al. (2011); Moseley et al. (2015, 2020), Antro del Corchia cave (CC5): Drysdale et al. (2005), Spannagel cave: Wendt et al. (2021).

Table 8
Comparison of midpoint ages of 65°N summer solstice insolation and $\delta^{18}O_{atm}$ on DF2021 gas age.

Midpoint of 65°N summer solstice insolation (kyr BP)	Midpoint of $\delta^{18}O_{atm}$ (kyr BP, DF2021 gas age)	Lag of $\delta^{18}O_{atm}$ to 65°N inso. at midpoint (kyr)	Deviation from the assumed lag of 5.9 kyr (kyr)
17.5	11.1	6.4	0.5
30.0	24.4	5.6	−0.3
53.0	48.7	4.3	−1.6
65.5	59.6	5.9	0.04
78.2	73.8	4.4	−1.5
89.7	85.8	3.9	−2.0
100.4	97.7	2.7	−3.2
110.6	109.2	1.4	−4.5
121.9	119.5	2.4	−3.5
133.5	129.4	4.1	−1.8
145.4	139.1	6.3	0.4
169.6	165.8	3.8	−2.1
181.5	178.4	3.1	−2.8
193.3	189.6	3.7	−2.2
203.9	200.0	3.9	−2.0

Fig. 11. Phasing between $\delta^{18}O_{atm}$ and 65°N summer solstice insolation. (a) $\delta^{18}O_{atm}$ of the DF core (Kawamura et al., 2007) on the DF2021 gas age scale with its filtered curve. (b) 65°N summer solstice insolation. Vertical lines in (a) and (b) indicate midpoints between maxima and minima. (c) Lag of $\delta^{18}O_{atm}$ behind 65°N summer solstice insolation for the midpoints. Horizontal red line indicates the constant lag of 5.9 kyr typically used for $\delta^{18}O_{atm}$-orbital age markers (Bazin et al., 2013). (d) IRD percentage at site ODP980 (brown: McManus et al., 1999), Ca/Sr ratio, an indicator of detrital carbonate, at site U1308 (black: Hodell et al., 2008) and detrital carbonate percentage at site 609/U1308 (blue: Obrochta et al., 2012, 2014). (For interpretation of the references to colour in this figure legend, the reader is referred to the Web version of this article.)

ring records using common signals such as volcanic signals and CH$_4$ concentrations, as well as cosmogenic radionuclides. (2) The new DF $\delta O_2/N_2$ data, which are not affected by gas-loss fractionation, are available and exhibit orbital-scale variations very similar to local summer insolation curve for the period older than 90 kyr BP. (3) Probabilistic dating methods have been developed to simultaneously optimize the ice and gas ages as well as accumulation rate, thinning and LID along depth. The model used here can incorporate various sources of chronological information, including age intervals between two layers to take into account correlated uncertainties. (4) Firn densification models have been advanced to produce thinner LID in glacial climates, to be consistent with data, which can provide reasonable prior LID and accumulation rate to the probabilistic model. The firn model is also integrated with the probabilistic dating model to produce a mutually consistent and physically sound chronology through the iterative method developed here. Our new chronology is tightly constrained by other well-dated records for the last 60 kyr, whereas it is independent from any other chronologies for the older period where the chronological constraints are sparce and different chronologies tend to disagree with each other.

The estimated uncertainty of DF2021 is smaller than ±0.05 and ± 0.9 kyr (2σ) for 0−30 and 30−60 kyr BP, respectively. For the last 60 kyr BP, DF2021 agrees well with the GICC05, WD2014 and U−Th chronology of speleothem within uncertainties. The largest age uncertainties of up to ±2.4 kyr for both ice and gas are observed between 60 and 90 kyr BP, where the chronology is only constrained by Δdepth from the bipolar-seesaw assumption (i.e., no absolute age markers). For the period older than 90 kyr BP, the uncertainty is relatively small (~0.5 kyr) at the $\delta O_2/N_2$ age markers, and it increases to ~1.3 kyr between the age markers.

Between 60 and 130 kyr BP, the timing of abrupt CH$_4$ shifts in the DF core agree within 1 kyr with those of NGRIP $\delta^{18}O$ on the GICC05modelext chronology as well as speleothem $\delta^{18}O$ from China and Europe on the U−Th chronologies, suggesting that the actual error is smaller than the estimated uncertainty for the 60−90 kyr BP range. The good agreements suggest that the assumption of zero phasing between the $\delta O_2/N_2$ record and local summer insolation is valid for the DF core at least for this age range. We also support the earlier suggestions that AICC2012 is too young around 110 kyr BP (the period including DO events 23−25). We attribute

the source of the age error to variable phasing of $\delta^{18}O_{atm}$ with respect to insolation.

Between 130 and 207 kyr BP, the degree of similarity between the variations of DF CH_4 and speleothem $\delta^{18}O$ is lower than in the last glacial period, making the comparison of the chronologies more challenging. However, we could identify eight events for the age comparisons and found that the agreements are reasonable considering the uncertainties of both DF2021 and U−Th chronologies (both are on the order of 1.5 kyr).

According to DF2021, the lag of $\delta^{18}O_{atm}$ midpoint behind that of 65°N summer solstice insolation is 6.4 kyr for the last deglaciation, which is significantly larger than the average of 4.1 ± 1.4 kyr over the last 207 kyr. On the other hand, the lags are significantly smaller than the average for the consecutive midpoints at 100.4, 110.6, and 121.9 kyr BP, indicating that the orbital tuning with $\delta^{18}O_{atm}$ may produce prolonged biases in the chronology. With the limitations, the phasing between $\delta^{18}O_{atm}$ and insolation clarified by our chronology would still be useful for future efforts of ice-core dating if other age constraints are weak or lacking, which might be the case for the "Oldest Ice Cores" (Fischer et al., 2013). In such cases, we suggest using the mean lag of $\delta^{18}O_{atm}$ behind 65°N summer solstice insolation of 4.1 ± 2.8 kyr (2 σ) kyr, and excluding the midpoints where the precessional amplitudes in the $\delta^{18}O_{atm}$ record are too small to precisely determine their positions, such as those around 42 and 150 kyr BP.

Future directions of the DF chronological developments may include the extension towards the older part of the core as new and unfractionated $\delta O_2/N_2$ data as well as high-precision $\delta^{15}N$ and CH_4 data become available, and the integration of the DF core or its chronological constraints to the multiple ice-core (or multiple paleoarchive) datings with the probabilistic approach.

Author contribution

Ikumi Oyabu: Conceptualization, Methodology, Formal analysis, Investigation, Writing - Original Draft, Visualization, Funding acquisition. **Kenji Kawamura:** Conceptualization, Methodology, Investigation, Writing - Original Draft, Supervision, Funding acquisition, **Christo Buizert:** Methodology, Software, Formal analysis, Writing - Review & Editing, **Frédéric Parrenin:** Methodology, Software, Formal analysis, Writing - Review & Editing, **Anais Orsi:** Methodology, Software, Formal analysis, Writing - Review &

Editing. **Kyotaro Kitamura:** Methodology, Investigation. **Shuji Aoki:** Methodology, Investigation. **Takakiyo Nakazawa:** Methodology, Investigation.

## Declaration of competing interest

Data availability

Acknowledgments

Appendix A

Fig. A1. All CH_4 concentration data from the DF core measured at different institutes and over different periods. Some data points (red crosses) are excluded for constructing the composite CH_4 record. See section 2.3.1 for the details of data selection.
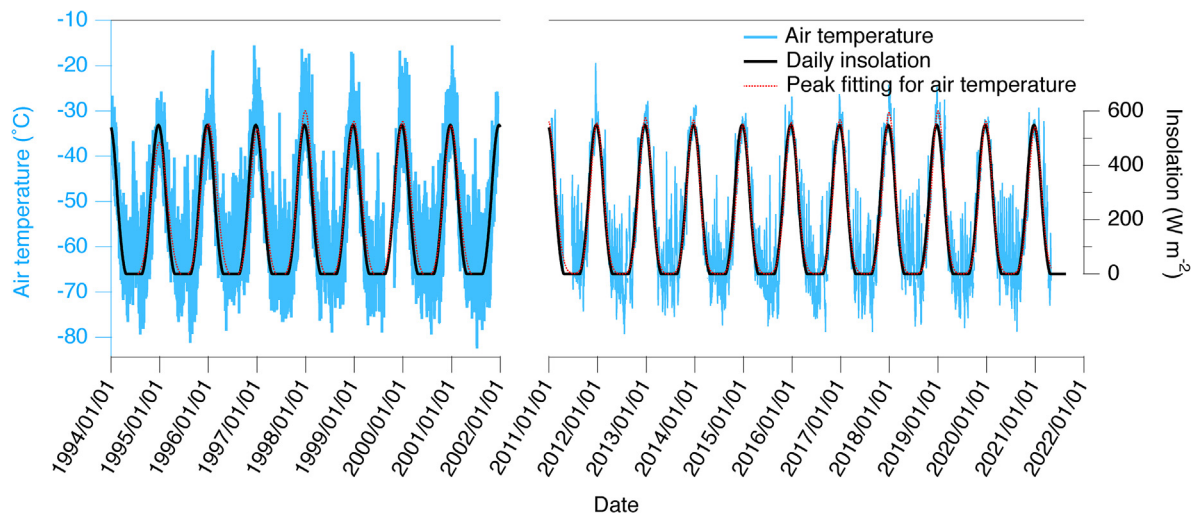
Fig. A2. Comparison between daily mean insolation (calculated with the AnalySeries software using the Laskar et al., 2004 solution) and air temperature observed by an automatic weather station (Takahashi et al., 2004; Morino et al., 2021) at Dome Fuji, Antarctica. A general peak fitting algorithm ("Multipeak Fitting 2" package of Igor Pro®) was used for identifying the timing of summer temperature peaks (see text).
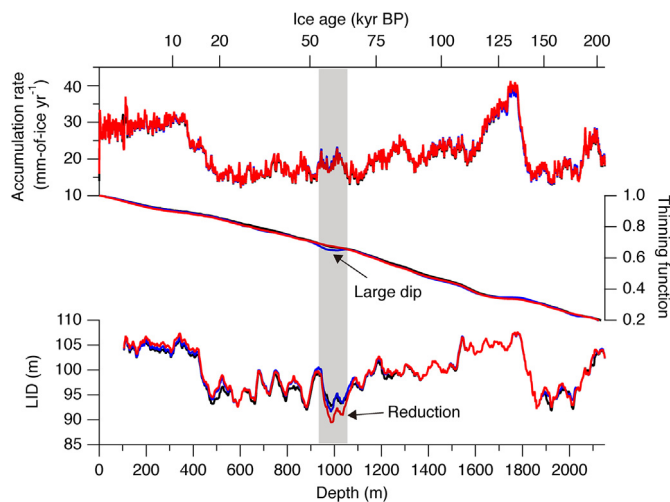

Fig. A3. Comparison between the *A*, τ, and LID with (red and blue) and without (black) Δdepth constraints for DO14, 16.1 and 17.1. If relatively large uncertainty of τ is assigned (before Step 2, increased linearly from the ice-sheet surface (0%) to the bottom (100%)), a large dip is produced in τ (blue). On the other hand, if the smaller uncertainty of τ (the result from Step 2) is assigned, shallowing of LID is produced (red).
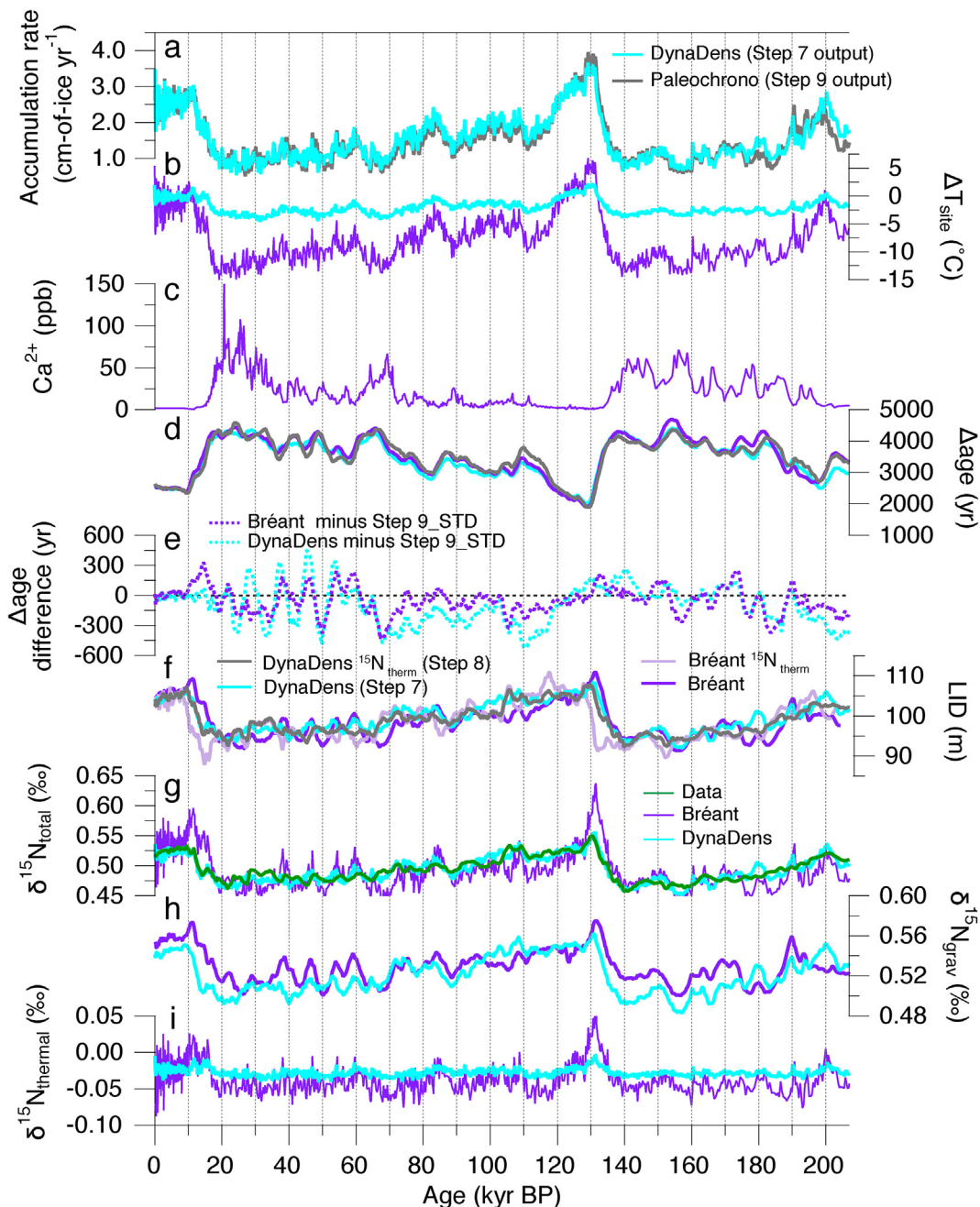
Fig. A4. Comparison between the results or inputs of DynaDens and Bréant firn densification model. (a) Optimized accumulation rate by DynaDens (light blue, after Step 7) and Paleochrono standard run (Step 9) (grey). (b) Optimized surface temperature by DynaDens (light blue) and Bréant model (purple). (c) Ca^{2+} concentration used for the Bréant model (Goto-Azuma et al., 2019). (d) Δage from Paleochrono (grey), DynaDens (light blue) and Bréant model (purple). (e) Difference of Δage between DynaDens and Paleochrono standard run (light blue), and that between Bréant model and Paleochrono standard run (purple). (f) LID from DynaDens model (light blue), Bréant model (purple), the $\delta^{15}N$ data corrected for the $\delta^{15}N_{therm}$ by DynaDens (grey), from the $\delta^{15}N$ data corrected for the $\delta^{15}N_{therm}$ by Bréant model (light purple), (g) $\delta^{15}N$ data and modeled $\delta^{15}N_{total}$ by DynaDens and Bréant model. (h) Gravitational component of $\delta^{15}N$ by DynaDens (light blue) and Bréant model (purple), (i) Thermal component of $\delta^{15}N$ by DynaDens (light blue) and Bréant model (purple) and Bréant model.
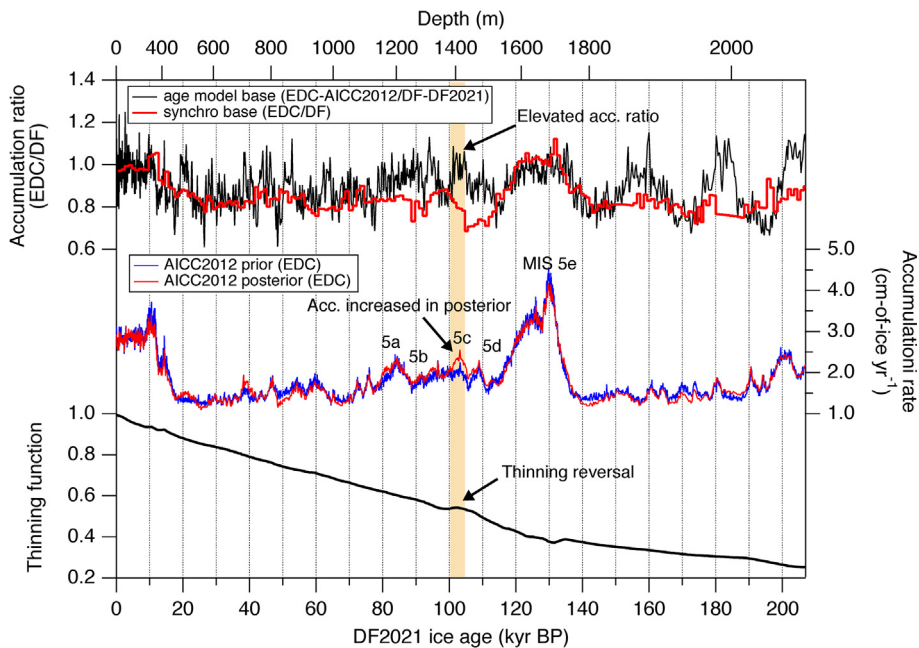
Fig. A5. Anomalous accumulation rate and thinning in the EDC core around 100 kyr BP from posteriors of AICC2012, as possible indicators for errors in δ¹⁸O_atm gas age markers. (a) Ratio of posterior of accumulation rate for the EDC core (from AICC2012, Veres et al., 2013; Bazin et al., 2013) to that for the DF core (from DF2021), and the ratio based on detailed age synchronization between the cores (Parrenin et al., 2016). (b) Accumulation of the prior (blue) and posterior (red) of the EDC core in the AICC2012 chronology (Parrenin et al., 2007b; Veres et al., 2013; Bazin et al., 2013). (c) Thinning function of the EDC core in the AICC2012 chronology (Veres et al., 2013; Bazin et al., 2013).

Appendix B. Validation of Δdepth for DO 20 by Toba volcanic matching

The bipolar ice-core signals of a Toba volcanic eruption (T9 event, ~76 kyr BP) found in the DF and NGRIP cores (Svensson et al., 2013) can be used to validate Δdepth at DO 20. The T9 event in the NGRIP core (2572.61 m) is located close to the onset of DO 20 (2579.13 m), and the temporal distance between the two layers is 403 years according to the GICC05modelext chronology. Thus, the ice depth for DO 20 in the DF core can be estimated using the T9 event in the DF core (1185.55 m) and the depth offset equivalent to the 403 years (between T9 and DO 20) from the depth-age scale

from Step 2 (Fig. B1a). The Δdepth for DO 20 thus estimated is 39.09 m, which agrees with that from the bipolar seesaw assumption (40.31 ± 1.40 m) within uncertainty (Fig. 5, B1b). Based on the following test, we also note that the replacement of Δdepth constraint for DO20 does not affect the resulting chronology. We replaced the Δdepth constraint at DO 20 with 39.09 m with 1 σ uncertainty of 0.7 m (equivalent to ~10% of the T9-DO 20 age difference), and kept all other constraints unchanged to run Paleochrono. The resulting ice and gas ages agree within 20 and 90 years, respectively, to the DF2021 chronology, with the reduction of age uncertainties around DO 20 by a few years only.
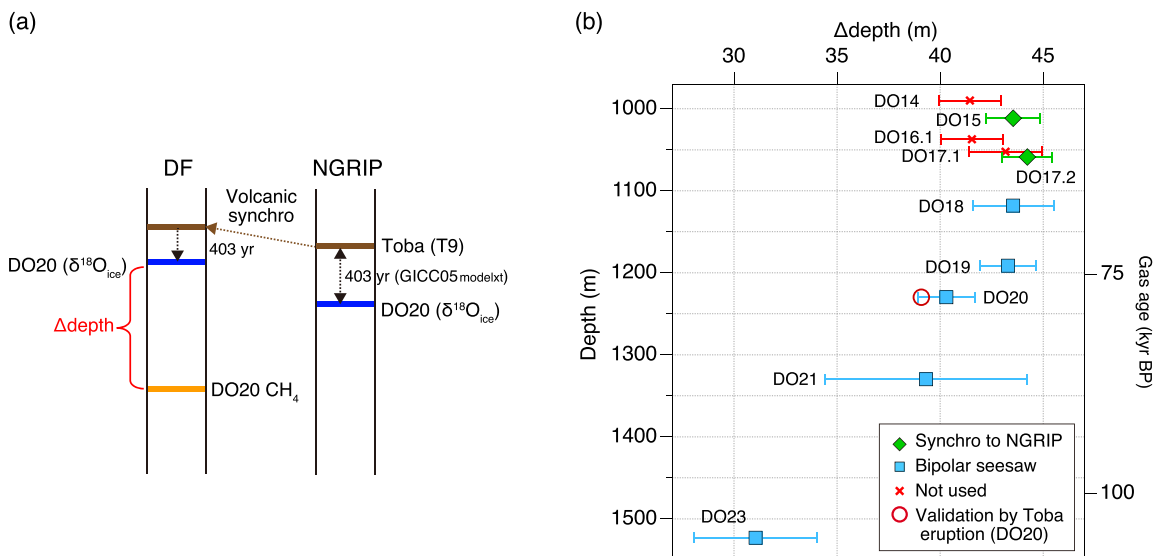
Fig. B1. (a) Schematic of Δdepth estimation for DO 20 based on Toba volcanic matching, and (b) enlarged view of Fig. 5.

References

Andersen, K.K., Svensson, A., Johnsen, S.J., Rasmussen, S.O., Bigler, M., Röthlisberger, R., Ruth, U., Siggaard-Andersen, M.-L., Peder Steffensen, J., Dahl-Jensen, D., Vinther, B., Clausen, H.B., 2006. The Greenland Ice Core Chronology 2005, 15–42ka. Part 1: constructing the time scale. Quat. Sci. Rev. 25, 3246–3257. https://doi.org/10.1016/j.quascirev.2006.08.002.

Barker, S., Knorr, G., Edwards, R.L., Parrenin, F., Putnam, A.E., Skinner, L.C., Wolff, E., Ziegler, M., 2011. 800,000 Years of abrupt climate variability. Science 334, 347–351. https://doi.org/10.1126/science.1203580.

Barnola, J.M., Pimienta, P., Raynaud, D., Korotkevich, Y.S., 1991. CO_2-climate relationship as deduced from the Vostok ice core: a re-examination based on new measurements and on a re-evaluation of the air dating. Tellus B 43, 83–90. https://doi.org/10.3402/tellusb.v43i2.15249.

Bazin, L., Landais, A., Capron, E., Masson-Delmotte, V., Ritz, C., Picard, G., Jouzel, J., Dumont, M., Leuenberger, M., Prié, F., 2016. Phase relationships between orbital forcing and the composition of air trapped in Antarctic ice cores. Clim. Past 12, 729–748. https://doi.org/10.5194/cp-12-729-2016.

Bazin, L., Landais, A., Lemieux-Dudon, B., Toyé Mahamadou Kele, H., Veres, D., Parrenin, F., Martinerie, P., Ritz, C., Capron, E.F.N., Lipenkov, V., Loutre, M.F., Raynaud, D., Vinther, B., Svensson, A., Rasmussen, S.O., Severi, M., Blunier, T., Leuenberger, M., Fischer, H., Masson-Delmotte, V., Chappellaz, J., Wolff, E., 2013. An optimized multi-proxy, multi-site Antarctic ice and gas orbital chronology (AICC2012): 120-800 ka. Clim. Past 9, 1715–1731. https://doi.org/10.5194/cp-9-1715-2013.

Bender, M., Sowers, T., Lipenkov, V., 1995. On the concentrations of O_2, N_2, and Ar in trapped gases from ice cores. J. Geophys. Res. 100, 18651–18660. https://doi.org/10.1029/94JD02212.

Bender, M.L., 2002. Orbital tuning chronology for the Vostok climate record supported by trapped gas composition. Earth Planet Sci. Lett. 204, 275–289. https://doi.org/10.1016/S0012-821X(02)00980-9.

Boch, R., Cheng, H., Lawrence Edwards, R., Wang, X., Häuselmann, P., 2011. NALPS: a precisely dated European climate record 120–60 ka. Clim. Past 7, 1247–1259. https://doi.org/10.5194/cp-7-1247-2011.

Bréant, C., Martinerie, P., Orsi, A., Arnaud, L., Landais, A., 2017. Modelling firn thickness evolution during the last deglaciation: constraints on sensitivity to temperature and impurities. Clim. Past 13, 833–853. https://doi.org/10.5194/cp-13-833-2017.

Buizert, C., Cuffey, K.M., Severinghaus, J.P., Baggenstos, D., Fudge, T.J., Steig, E.J., Markle, B.R., Winstrup, M., Rhodes, R.H., Brook, E.J., Sowers, T.A., Clow, G.D., Cheng, H., Edwards, R.L., Sigl, M., McConnell, J.R., Taylor, K.C., 2015. The WAIS Divide deep ice core WD2014 chronology -Part 1: methane synchronization (68–31 ka BP) and the gas age–ice age difference. Clim. Past 11, 153–173. https://doi.org/10.5194/cp-11-153-2015.

Buizert, C., Sigl, M., Severi, M., Markle, B.R., Wettstein, J.J., McConnell, J.R., Pedro, J.B., Sodemann, H., Goto-Azuma, K., Kawamura, K., Fujita, S., Motoyama, H., Hirabayashi, M., Uemura, R., Stenni, B., Parrenin, F., He, F., Fudge, T.J., Steig, E.J., 2018. Abrupt ice-age shifts in southern westerly winds and Antarctic climate forced from the north. Nature 563, 681–685. https://doi.org/10.1038/s41586-018-0727-5.

Buizert, C., Fudge, T.J., Roberts, W.H.G., Steig, E.J., Sherriff-Tadano, S., Ritz, C., Lefebvre, E., Edwards, J., Kawamura, K., Oyabu, I., Motoyama, H., Kahle, E.C., Jones, T.R., Abe-Ouchi, A., Obase, T., Martin, C., Corr, H., Severinghaus, J.P., Beaudette, R., Epifanio, J.A., Brook, E.J., Martin, K., Chappellaz, J., Aoki, S., Nakazawa, T., Sowers, T., Alley, R., Ahn, J., Sigl, M., Severi, M., Dunbar, N.W., Svensson, A., Fegyveresi, J., He, C., Liu, Z., Zhu, J., Otto-Bliesner, B., Lipenkov, V., Kageyama, M., Schwander, J., 2021. Antarctic-wide surface temperature and elevation during the last glacial maximum. Science 372, 1097–1101. https://doi.org/10.1126/science.abd2897.

Buizert, C., 2021. The ice core gas age-ice age difference as a proxy for surface temperature. Geophys. Res. Lett. 48 (20), e2021GL094241. https://doi.org/10.1029/2021GL094241.

Chen, S., Wang, Y., Cheng, H., Edwards, R.L., Wang, X., Kong, X., Liu, D., 2016. Strong coupling of Asian Monsoon and Antarctic climates on sub- orbital timescales. Sci. Rep. 1–7. https://doi.org/10.1038/srep32995.

Cheng, H., Edwards, R.L., Broecker, W.S., Denton, G.H., Kong, X., Wang, Y., Zhang, R., Wang, X., 2009. Ice age terminations. Science 326, 248–252. https://doi.org/10.1126/science.1177840.

Cheng, H., Edwards, R.L., Sinha, A., Spötl, C., Yi, L., Chen, S., Kelly, M., Kathayat, G., Wang, X., Li, X., Kong, X., Wang, Y., Ning, Y., Zhang, H., 2016. The Asian monsoon over the past 640,000 years and ice age terminations. Nature 534, 640–646. https://doi.org/10.1038/nature18591.

Cole-Dai, J., 2014a. Major Ion Chemistry Data of WAIS Divide Ice Core Brittle Ice. https://doi.org/10.7265/N5RF5S0D.

Cole-Dai, J., 2014b. Major Ion Concentrations in WDC05Q and WDC06A Ice Cores (WAIS Divide). U.S. Antarctic Program. https://doi.org/10.7265/N54M92H3.

Crowley, T.J., 1992. North Atlantic deep water cools the southern hemisphere. Paleoceanography 7 (4), 489–497. https://doi.org/10.1029/92PA01058.

Dansgaard, W., Johnsen, S.J., 1969. A flow model and a time scale for the ice core from Camp Century, Greenland. J. Glaciol. 8, 215–223. https://doi.org/10.3189/S0022143000031208.

Dome Fuji Ice Core Project Members, Kawamura, K., Abe-Ouchi, A., Motoyama, H., Ageta, Y., Aoki, S., Azuma, N., Fujii, Y., Fujita, K., Fujita, S., Fukui, K., Furukawa, T., Furusaki, A., Goto-Azuma, K., Greve, R., Hirabayashi, M., Hondoh, T., Hori, A.,

Horikawa, S., Horiuchi, K., Igarashi, M., Iizuka, Y., Kameda, T., Kanda, H., Kohno, M., Kuramoto, T., Matsushi, Y., Miyahara, M., Miyake, T., Miyamoto, A., Nagashima, Y., Nakayama, Y., Nakazawa, T., Nakazawa, F., Nishio, F., Obinata, I., Ohgaito, R., Oka, A., Okuno, J.i., Sakurai, T., Oyabu, I., Parrenin, F., Pattyn, F., Saito, F., Saito, T., Saito, T., Sakurai, T., Sasa, K., Seddik, H., Shibata, Y., Shinbori, K., Suzuki, K., Suzuki, T., Takahashi, A., Takahashi, K., Takahashi, S., Takata, M., Tanaka, Y., Uemura, R., Watanabe, G., Watanabe, O., Yamasaki, T., Yokoyama, K., Yoshimori, M., Yoshimoto, T., 2017. State dependence of climatic instability over the past 720,000 years from Antarctic ice cores and climate modeling. Sci. Adv. 3, e1600446. https://doi.org/10.1126/sciadv.1600446.

Dreyfus, G.B., Parrenin, F., Lemieux-Dudon, B., Durand, G., Masson-Delmotte, V., Jouzel, J., Barnola, J.M., Panno, L., Spahni, R., Tisserand, A., Siegenthaler, U., Leuenberger, M., 2007. Anomalous flow below 2700 m in the EPICA Dome C ice core detected using δ18O of atmospheric oxygen measurements. Clim. Past 3, 341–353. https://doi.org/10.5194/cp-3-341-2007.

Drysdale, R.N., Zanchetta, G., Hellstrom, J.C., Fallick, A.E., Zhao, J., 2005. Stalagmite evidence for the onset of the Last Interglacial in southern Europe at 129 ± 1 ka. Geophys. Res. Lett. 32, L24708. https://doi.org/10.1029/2005GL024658.

Drysdale, R.N., Zanchetta, G., Hellstrom, J.C., Fallick, A.E., McDonald, J., Cartwright, I., 2007. Stalagmite evidence for the precise timing of North Atlantic cold events during the early last glacial. Geol. 35, 77–80. https://doi.org/10.1130/G23161A.1.

Extier, T., Landais, A., Bréant, C., Prié, F., Bazin, L., Dreyfus, G., Roche, D.M., Leuenberger, M., 2018. On the use of δ18Oatm for ice core dating. Quat. Sci. Rev. 185, 244–257. https://doi.org/10.1016/j.quascirev.2018.02.008.

Fischer, H., Severinghaus, J., Brook, E., Wolff, E., Albert, M., Alemany, O., Arthern, R., Bentley, C., Blankenship, D., Chappellaz, J., Creyts, T., Dahl-Jensen, D., Dinn, M., Frezzotti, M., Fujita, S., Gallee, H., Hindmarsh, R., Hudspeth, D., Jugie, G., Kawamura, K., Lipenkov, V., Miller, H., Mulvaney, R., Parrenin, F., Pattyn, F., Ritz, C., Schwander, J., Steinhage, D., van Ommen, T., Wilhelms, F., 2013. Where to find 1.5 million yr old ice for the IPICS "Oldest-Ice" ice core. Clim. Past 9, 2489–2505. https://doi.org/10.5194/cp-9-2489-2013.

Fujita, S., Okuyama, J., Hori, A., Hondoh, T., 2009. Metamorphism of stratified firn at Dome Fuji, Antarctica: a mechanism for local insolation modulation of gas transport conditions during bubble close off. J. Geophys. Res. 114. https://doi.org/10.1029/2008JF001143.

Fujita, S., Parrenin, F., Severi, M., Motoyama, H., Wolff, E.W., 2015. Volcanic synchronization of Dome Fuji and Dome C Antarctic deep ice cores over the past 216 kyr. Clim. Past 11, 1395–1416. https://doi.org/10.5194/cp-11-1395-2015.

Goto-Azuma, K., Hirabayashi, M., Motoyama, H., Miyake, T., Kuramoto, T., Uemura, R., Igarashi, M., Iizuka, Y., Sakurai, T., Horikawa, S., Suzuki, K., Suzuki, T., Fujita, K., Kondo, Y., Hattori, S., Fujii, Y., 2019. Reduced marine phytoplankton sulphur emissions in the Southern Ocean during the past seven glacials. Nat. Commun. 10. https://doi.org/10.1038/s41467-019-11128-6.

Herron, M.M., Langway, C.C., 1980. Firn densification - an empirical-model. J. Glaciol. 25, 373–385. https://doi.org/10.3189/S0022143000015239.

Hodell, D.A., Channell, J.E.T., Curtis, J.H., Romero, O.E., Röhl, U., 2008. Onset of "Hudson strait" Heinrich events in the eastern North Atlantic at the end of the middle pleistocene transition (~640 ka)? Paleoceanography 23 (4), PA4218. https://doi.org/10.1029/2008PA001591.

Horiuchi, K., Uchida, T., Sakamoto, Y., Ohta, A., Matsuzaki, H., Shibata, Y., Motoyama, H., 2008. Ice core record of ^{10}Be over the past millennium from Dome Fuji, Antarctica: a new proxy record of past solar activity and a powerful tool for stratigraphic dating. Quat. Geochronol. 3, 253–261. https://doi.org/10.1016/j.quageo.2008.01.003.

Ikeda-Fukazawa, T., Hondoh, T., Fukumura, T., Fukazawa, H., Mae, S., 2001. Variation in N_2/O_2 ratio of occluded air in Dome Fuji antarctic ice. J. Geophys. Res. 106, 17799–17810. https://doi.org/10.1029/2000JD000104.

Ikeda-Fukazawa, T., Fukumizu, K., Kawamura, K., Aoki, S., Nakazawa, T., Hondoh, T., 2005. Effects of molecular diffusion on trapped gas composition in polar ice cores. Earth Planet Sci. Lett. 229, 183–192. https://doi.org/10.1016/j.epsl.2004.11.011.

Johnsen, S.J., Dahl-Jensen, D., Gundestrup, N., Steffensen, J.P., Clausen, H.B., Miller, H., Masson-Delmotte, V., Sveinbjörnsdóttir, Á.E., White, J., 2001. Oxygen isotope and palaeotemperature records from six Greenland ice-core stations: camp Century, Dye-3, GRIP, GISP2, Renland and NorthGRIP. J. Quat. Sci. 16, 299–307. https://doi.org/10.1002/jqs.622.

Jouzel, J., Masson-Delmotte, V., Cattani, O., Dreyfus, G., Falourd, S., Hoffmann, G., Minster, B., Nouet, J., Barnola, J.M., Chappellaz, J., Fischer, H., Gallet, J.C., Johnsen, S., Leuenberger, M., Loulergue, L., Luethi, D., Oerter, H., Parrenin, F., Raisbeck, G., Raynaud, D., Schilt, A., Schwander, J., Selmo, E., Souchez, R., Spahni, R., Stauffer, B., Steffensen, J.P., Stenni, B., Stocker, T.F., Tison, J.L., Werner, M., Wolff, E.W., 2007. Orbital and millennial antarctic climate variability over the past 800,000 years. Science 317, 793–796. https://doi.org/10.1126/science.1141038.

Kanzawa, K., Miyake, F., Horiuchi, K., Sasa, K., Takano, K., Matsumura, M., Takahashi, T., Motizuki, Y., Takahashi, K., Nakai, Y., Ohtani, K., Tada, Y., Ochiai, Y., Motoyama, H., Matsuzaki, H., Yamazaki, A., Muramatsu, Y., Yamagata, T., 2021. High-resolution 10Be and 36Cl data from the antarctic Dome Fuji ice core (~100 Years around 5480 BCE): an unusual grand solar minimum occurrence? J. Geophys. Res.: Space Phys. 126, e2021JA029378. https://doi.org/10.1029/2021JA029378.

Kawamura, K., 2001. Variations of Atmospheric Components over the Past 340000 Years from Dome Fuji Deep Ice Core. Ph. D thesis, Tohoku University, Antarctica. http://hdl.handle.net/10097/38833.

Kawamura, K., Nakazawa, T., Aoki, S., Fujii, Y., Watanabe, O., Severinghaus, J.P., 2004.

Close Resemblance between Local Summer Insolation, O_2/N_2 and Total Air Content from the Dome Fuji Ice Core, Antarctica. American Geophysical Union, Fall Meeting 2004 abstract id. C33C-0356.

Kawamura, K., Nakazawa, T., Aoki, S., Sugawara, S., Fujii, Y., Watanabe, O., 2003. Atmospheric CO_2 variations over the last three glacial-interglacial climatic cycles deduced from the Dome Fuji deep ice core, Antarctica using a wet extraction technique. Tellus B 55, 126–137. https://doi.org/10.1034/j.1600-0889.2003.00050.x.

Kawamura, K., Severinghaus, J.P., Ishidoya, S., Sugawara, S., Hashida, G., Motoyama, H., Fujii, Y., Aoki, S., Nakazawa, T., 2006. Convective mixing of air in firn at four polar sites. Earth Planet Sci. Lett. 244, 672–682. https://doi.org/10.1016/j.epsl.2006.02.017.

Kawamura, K., Parrenin, F., Lisiecki, L., Uemura, R., Vimeux, F., Severinghaus, J.P., Hutterli, M.A., Nakazawa, T., Aoki, S., Jouzel, J., Raymo, M.E., Matsumoto, K., Nakata, H., Motoyama, H., Fujita, S., Goto-Azuma, K., Fujii, Y., Watanabe, O., 2007. Northern Hemisphere forcing of climatic cycles in Antarctica over the past 360,000years. Nature 448, 912–916. https://doi.org/10.1038/nature06015.

Kelly, M.J., 2010. Characterization of Asian Monsoon Variability since the Penultimate Interglacial on Orbital and Sub-orbital Timescales, Dongge Cave, China, Ph. D Thesis. The University of Minnesota, USA. https://hdl.handle.net/11299/59287.

Kelly, M.J., Edwards, R.L., Cheng, H., Yuan, D., Cai, Y., Zhang, M., Lin, Y., An, Z., 2006. High resolution characterization of the Asian Monsoon between 146,000 and 99,000 years B.P. from Dongge Cave, China and global correlation of events surrounding Termination II. Palaeogeogr. Palaeoclimatol. Palaeoecol. 236, 20–38. https://doi.org/10.1016/j.palaeo.2005.11.042.

Landais, A., Dreyfus, G., Capron, E., Pol, K., Loutre, M.F., Raynaud, D., Lipenkov, V.Y., Arnaud, L., Masson-Delmotte, V., Paillard, D., Jouzel, J., Leuenberger, M., 2012. Towards orbital dating of the EPICA Dome C ice core using $\delta O_2/N_2$. Clim. Past 8, 191–203. https://doi.org/10.5194/cp-8-191-2012.

Laskar, J., Rovbutel, P., Joutel, F., Gastineau, M., Correia, A.C.M., Levrard, B., 2004. A long-term numerical solution for the insolation quantities of the Earth. A & A 428, 261–285. https://doi.org/10.1051/0004-6361:20041335.

Lemieux-Dudon, B., Blayo, E., Petit, J.-R., Waelbroeck, C., Svensson, A., Ritz, C., Barnola, J.-M., Narcisi, B.M., Parrenin, F., 2010. Consistent dating for Antarctic and Greenland ice cores. Quat. Sci. Rev. 29, 8–20. https://doi.org/10.1016/j.quascirev.2009.11.010.

Lipenkov, V.Y., Raynaud, D., Loutre, M.F., 2011. On the potential of coupling air content and O_2/N_2 from trapped airfor establishing an ice core chronology tuned on local insolation. Quat. Sci. Rev. 30, 3280–3289. https://doi.org/10.1016/j.quascirev.2011.07.013.

Loulergue, L., Schilt, A., Spahni, R., Masson-Delmotte, V., Blunier, T., Lemieux, B., Barnola, J.-M., Raynaud, D., Stocker, T.F., Chappellaz, J., 2008. Orbital and millennial-scale features of atmospheric CH_4 over the past 800,000years. Nature 453, 383–386. https://doi.org/10.1038/nature06950.

Lüthi, D., Bereiter, B., Stauffer, B., Winkler, R., Schwander, J., Kindler, P., Leuenberger, M., Kipfstuhl, J., Capron, E., Landais, A., Fischer, H., Stocker, T.F., 2010. CO_2 and O_2/N_2 variations in and just below the bubble–clathrate transformation zone of Antarctic ice cores. Earth Planet Sci. Lett. 297, 226–233. https://doi.org/10.1016/j.epsl.2010.06.023.

McConnell, J., 2017. WAIS Divide Ice-Core Aerosol Records from 1300 to 3404 M. U.S. Antarctic Program. https://doi.org/10.15784/601008.

McManus, J.F., Oppo, D.W., Cullen, J.L., 1999. A 0.5-million-year record of millennial-scale climate variability in the North Atlantic. Science 283 (5404), 971–975. https://doi.org/10.1126/science.283.5404.971.

Martinerie, P., Lipenkov, V.Y., Raynaud, D., Chappellaz, J., Barkov, N.I., Lorius, C., 1994. Air content paleo record in the Vostok ice core (Antarctica): a mixed record of climatic and glaciological parameters. J. Geophys. Res. 99 (D5). https://doi.org/10.1029/93jd03223.

Miyake, F., Horiuchi, K., Motizuki, Y., Nakai, Y., Takahashi, K., Masuda, K., Motoyama, H., Matsuzaki, H., 2019. 10Be signature of the cosmic ray event in the 10th century CE in both hemispheres, as confirmed by quasi-annual 10Be data from the antarctic Dome Fuji ice core. Geophys. Res. Lett. 46, 11–18. https://doi.org/10.1029/2018GL080475.

Miyake, F., Suzuki, A., Masuda, K., Horiuchi, K., Motoyama, H., Matsuzaki, H., Motizuki, Y., Takahashi, K., Nakai, Y., 2015. Cosmic ray event of A.D. 774–775 shown in quasi-annual 10Be data from the Antarctic Dome Fuji ice core. Geophys. Res. Lett. 42, 84–89. https://doi.org/10.1002/2014GL062218.

Morino, S., Kurita, N., Hirasawa, N., Motoyama, H., Sugiura, K., Lazzara, M.A., Mikolajczyk, D., Welhouse, L., Keller, L., Weidner, G., 2021. Comparison of ventilated and unventilated air temperature measurements in inland dronning maud land on the East Antarctic plateau. J. Atmos. Ocean. Technol. 2061–2070. https://doi.org/10.1175/JTECH-D-21-0107.1.

Moseley, G.E., Spötl, C., Brandstätter, S., Erhardt, T., Luetscher, M., Edwards, R.L., 2020. NALPS19: sub-orbital-scale climate variability recorded in northern Alpine speleothems during the last glacial period. Clim. Past 16, 29–50. https://doi.org/10.5194/cp-16-29-2020.

Moseley, G.E., Spötl, C., Cheng, H., Boch, R., Min, A., Lawrence Edwards, R., 2015. Termination-II interstadial/stadial climate change recorded in two stalagmites from the north European Alps. Quat. Sci. Rev. 127, 229–239. https://doi.org/10.1016/j.quascirev.2015.07.012.

Motizuki, Y., Nakai, Y., Takahashi, K., Igarashi, M., Motoyama, H., Suzuki, K., 2014. Dating of a Dome Fuji (Antarctica) shallow ice core by volcanic signal synchronization with B32 and EDML1 chronologies. Cryosphere Discuss. 8, 769–804. https://doi.org/10.5194/tcd-8-769-2014.

Motoyama, H., 2007. The second deep ice coring project at Dome Fuji, Antarctica. Sci. Drill. 5, 41–43. https://doi.org/10.5194/sd-5-41-2007.

Motoyama, H., Takahashi, A., Tanaka, Y., Shinbori, K., Miyahara, M., Yoshimoto, T., Fujii, Y., Furusaki, A., Azuma, N., Ozawa, Y., Kobayashi, A., Yoshie, Y., 2021. Deep ice core drilling to a depth of 3035.22 m at Dome Fuji, Antarctica in 2001-07. Ann. Glaciol. 212–222. https://doi.org/10.1017/aog.2020.84.

Nakano, S., Suzuki, K., Kawamura, K., Parrenin, F., Higuchi, T., 2016. A sequential Bayesian approach for the estimation of the age-depth relationship of the Dome Fuji ice core. Nonlinear Process Geophys. 23, 31–44. https://doi.org/10.5194/npg-23-31-2016.

Nakazawa, T., Machida, T., Esumi, K., Tanaka, M., Fujii, Y., Aoki, S., Watanabe, O., 1993. Measuretnents of CO_2 and CH_4 concentrations a polar ice core. J. Glaciol. 39, 209–215. https://doi.org/10.3189/S0022143000015860.

Obrochta, S.P., Miyahara, H., Yokoyama, Y., Crowley, T.J., 2012. A re-examination of evidence for the North Atlantic "1500-year cycle" at Site 609. Quat. Sci. Rev. 55, 23–33. https://doi.org/10.1016/j.quascirev.2012.08.008.

North Greenland Ice Core Project members, 2004. High-resolution record of Northern Hemisphere climate extending into the last interglacial period. Nature 431, 147–151. https://doi.org/10.1038/nature02805.

Obrochta, S.P., Crowley, T.J., Channell, J.E.T., Hodell, D.A., Baker, P.A., Seki, A., Yokoyama, Y., 2014. Climate variability and ice-sheet dynamics during the last three glaciations. Earth Planet Sci. Lett. 406, 198–212. https://doi.org/10.1016/j.epsl.2014.09.004.

Oyabu, I., Kawamura, K., Uchida, T., Fujita, S., Kitamura, K., Hirabayashi, M., Aoki, S., Morimoto, S., Nakazawa, T., Severinghaus, J.P., Morgan, J., 2021. Fractionation of O_2/N_2 and Ar/N_2 in the Antarctic ice sheet during bubble formation and bubble–clathrate hydrate transition from precise gas measurements of the Dome Fuji ice core. Cryosphere 15, 5529–5555. https://doi.org/10.5194/tc-15-5529-2021.

Oyabu, I., Kawamura, K., Kitamura, K., Dallmayr, R., Kitamura, A., Sawada, C., Severinghaus, J.P., Beaudette, R., Orsi, A., Sugawara, S., Ishidoya, S., Dahl-Jensen, D., Goto-Azuma, K., Aoki, S., Nakazawa, T., 2020. New technique for high-precision, simultaneous measurements of CH_4, N_2O and CO_2 concentrations, isotopic and elemental ratios of N_2, O_2 and Ar, and total air content in ice cores by wet extraction. Atmos. Meas. Tech. 13, 6703–6731. https://doi.org/10.5194/amt-13-6703-2020.

Oyabu, I., Kawamura, K., Buizert, C., Parrenin, F., Orsi, A., Kitamura, K., Aoki, S., Nakazawa, T., 2022. DF2021 Chronology and Dome Fuji Gas Data (O_2/N_2, $d^{15}N$, CH_4) (0 - 207 Kyr BP), 1.00, Arctic Data Archive System (ADS). https://doi.org/10.17592/001.2022061303.

Paillard, D., Labeyrie, L., Yiou, P., 1996. Macintosh program performs time-series analysis. Eos, Transact. Am. Geophys. Union, (AGU) 77, 379. https://doi.org/10.1029/96EO00259.

Parrenin, F., Jouzel, J., Waelbroeck, C., Ritz, C., Barnola, J.-M., 2001. Dating the Vostok ice core by an inverse method. J. Geophys. Res.: Atmosphere 106, 31837–31851. https://doi.org/10.1029/2001JD900245.

Parrenin, F., Bazin, L., Capron, E., Landais, A., Lemieux-Dudon, B., Masson-Delmotte, V., 2015. IceChrono1: a probabilistic model to compute a common and optimal chronology for several ice cores. Geosci. Model Dev. (GMD) 8, 1473–1492. https://doi.org/10.5194/gmd-8-1473-2015.

Parrenin, F., Barker, S., Blunier, T., Chappellaz, J., Jouzel, J., Landais, A., Masson-Delmotte, V., Schwander, J., Veres, D., 2012. On the gas-ice depth difference (Δdepth) along the EPICA Dome C ice core. Clim. Past 8, 1239–1255. https://doi.org/10.5194/cp-8-1239-2012.

Parrenin, F., Fujita, S., Abe-Ouchi, A., Kawamura, K., Masson-Delmotte, V., Motoyama, H., Saito, F., Severi, M., Stenni, B., Uemura, R., Wolff, E.W., 2016. Climate dependent contrast in surface mass balance in East Antarctica over the past 216 ka. J. Glaciol. 62, 1037–1048. https://doi.org/10.1017/jog.2016.85.

Parrenin, F., Bazin, L., Buizert, C., Capron, E., Beeman, J.C., Corrick, E.C., Drysdale, R.N., Kawamura, K., Landais, A., Mulvaney, R., Oyabu, I., Rasmussen, S.O., 2021. The Paleochrono probabilistic model to derive a consistent chronology for several paleoclimatic sites. EGU General Assem. https://doi.org/10.5194/egusphere-egu21-822 online, 19–30 Apr 2021 EGU21-822 2021.

Parrenin, F., Dreyfus, G., Durand, G., Fujita, S., Gagliardini, O., Gillet, F., Jouzel, J., Kawamura, K., Lhomme, N., Masson-Delmotte, V., Ritz, C., Schwander, J., Shoji, H., Uemura, R., Watanabe, O., Yoshida, N., 2007a. 1-D-ice flow modelling at EPICA Dome C and Dome Fuji, East Antarctica. Clim. Past 3, 243–259. https://doi.org/10.5194/cp-3-243-2007.

Parrenin, F., Barnola, J.M., Beer, J., Blunier, T., Castellano, E., Chappellaz, J., Dreyfus, G., Fischer, H., Fujita, S., Jouzel, J., Kawamura, K., Lemieux-Dudon, B., Loulergue, L., Masson-Delmotte, V., Narcisi, B., Petit, J.R., Raisbeck, G., Raynaud, D., Ruth, U., Schwander, J., Severi, M., Spahni, R., Steffensen, J.P., Svensson, A., Udisti, R., Waelbroeck, C., Wolff, E., 2007b. The EDC3 chronology for the EPICA Dome C ice core. Clim. Past 3, 485–497. https://doi.org/10.5194/cp-3-485-2007.

Parrenin, F., Rémy, F., Ritz, C., Siegert J., M., Jouzel, J., 2004. New modeling of the Vostok ice flow line and implication for the glaciological chronology of the Vostok ice core. J. Geophys. Res. 109. https://doi.org/10.1029/2004JD004561.

Petit, J.R., Jouzel, J., Raynaud, D., Barkov, N.I., Barnola, J.-M., Basile, I., Bender, M., Chappellaz, J., Davis, M., Delaygue, G., Delmotte, M., Kotlyakov, V.M., Legrand, M., Lipenkov, V.Y., Lorius, C., Pépin, L., Ritz, C., Saltzman, E., Stievenard, M., 1999. Climate and atmospheric history of the past 420,000 years from the Vostok ice core, Antarctica. Nature 399 (6735), 429–436. https://doi.org/10.1038/20859.

Rasmussen, S.O., Andersen, K.K., Svensson, A.M., Steffensen, J.P., Vinther, B.M.,

Clausen, H.B., Siggaard-Andersen, M.L., Johnsen, S.J., Larsen, L.B., Dahl-Jensen, D., Bigler, M., Röthlisberger, R., Fischer, H., Goto-Azuma, K., Hansson, M.E., Ruth, U., 2006. A new Greenland ice core chronology for the last glacial termination. J. Geophys. Res.: Atmosphere 111. https://doi.org/10.1029/2005JD006079.

Rasmussen, S., Bigler, M., Blockley, S.P., Blunier, T., Buchardt, S.L., Clausen, H.B., Cvijanovic, I., Dahl-Jensen, D., Johnsen, S.J., Fischer, H., Gkinis, V., Guillevic, M., Hoek, W.Z., Lowe, J.J., Pedro, J.B., Popp, T., Seierstad, I.K., Steffensen, J.P., Svensson, A.M., Vallelonga, P., Vinther, B.M., Walker, M.J.C., Wheatley, J.J., Winstrup, M., 2014. A stratigraphic framework for abrupt climatic changes during the Last Glacial period based on three synchronized Greenland ice-core records: refining and extending the INTIMATE event stratigraphy. Quat. Sci. Rev. 106, 14–28. https://doi.org/10.1016/j.quascirev.2014.09.007.

Raynaud, D., Lipenkov, V., Lemieux-Dudon, B., Duval, P., Loutre, M.-F., Lhomme, N., 2007. The local insolation signature of air content in Antarctic ice. A new step toward an absolute dating of ice records. Earth Planet Sci. Lett. 261, 337–349. https://doi.org/10.1016/j.epsl.2007.06.025.

Rhodes, R.H., Brook, E.J., Chiang, J.C.H., Blunier, T., 2015. Enhanced tropical methane production in response to iceberg discharge in the North Atlantic. Science 348, 1016–1019. https://doi.org/10.1126/science.1262005 2015.

Ruddiman, W.F., Raymo, M.E., 2003. A methane-based time scale for Vostok ice. Quat. Sci. Rev. 22, 141–155. https://doi.org/10.1016/S0277-3791(02)00082-3.

Schwander, J., 1989. The Transformation of Snow to Ice and the Occlusion of Gases, the Environmental Record in Glaciers and Ice Sheets. John Wiley, New York.

Severinghaus, J.P., Sowers, T., Brook, E., Alley, R.B., Bender, M., 1998. Timing of abrupt climate change at the end of the Younger Dryas interval from thermally fractionated gases in polar ice. Nature 391, 141–146. https://doi.org/10.1038/34346.

Severinghaus, J.P., Battle, M.O., 2006. Fractionation of gases in polar ice during bubble close-off: new constraints from firn air Ne, Kr and Xe observations. Earth Planet Sci. Lett. 244, 474–500. https://doi.org/10.1016/j.epsl.2006.01.032.

Shackleton, N.J., 2000. The 100,000-year ice-age cycle identified and found to lag temperature, carbon dioxide, and orbital eccentricity. Science 289, 1897–1902. https://doi.org/10.1126/science.289.5486.1897.

Shin, J., Nehrbass-Ahles, C., Grilli, R., Chowdhry Beeman, J., Parrenin, F., Teste, G., Landais, A., Schmidely, L., Silva, L., Schmitt, J., Bereiter, B., Stocker, T.F., Fischer, H., Chappellaz, J., 2020. Millennial-scale atmospheric CO_2 variations during the Marine Isotope Stage 6 period (190–135 ka). Clim. Past 16, 2203–2219. https://doi.org/10.5194/cp-16-2203-2020.

Sigl, M., Fudge, T.J., Winstrup, M., Cole-Dai, J., Ferris, D., McConnell, J.R., Taylor, K.C., Welten, K.C., Woodruff, T.E., Adolphi, F., Bisiaux, M., Brook, E.J., Buizert, C., Caffee, M.W., Dunbar, N.W., Edwards, R., Geng, L., Iverson, N., Koffman, B., Layman, L., Maselli, O.J., McGwire, K., Muscheler, R., Nishiizumi, K., Pasteris, D.R., Rhodes, R.H., Sowers, T.A., 2016. The WAIS Divide deep ice core WD2014 chronology — Part 2: annual-layer counting (0–31 ka BP). Clim. Past 12, 769–786. https://doi.org/10.5194/cp-12-769-2016.

Sime, L.C., Wolff, E.W., Oliver, K.I.C., Tindall, J.C., 2009. Evidence for warmer interglacials in East Antarctic ice cores. Nature 342–345. https://doi.org/10.1038/nature08564.

Sowers, T., Bender, M., Raynaud, D., 1989. Elemental and isotopic composition of occluded O_2 and N_2 in polar ice. J. Geophys. Res. 94, 5137–5150. https://doi.org/10.1029/JD094iD04p05137.

Stocker, T.F., Johnsen, S.J., 2003. A minimum thermodynamic model for the bipolar seesaw. Paleoceanography 18 (4). https://doi.org/10.1029/2003PA000920.

Suwa, M., Bender, M.L., 2008. Chronology of the Vostok ice core constrained by O_2/N_2 ratios of occluded air, and its implication for the Vostok climate records. Quat. Sci. Rev. 27, 1093–1106. https://doi.org/10.1016/j.quascirev.2008.02.017.

Svensson, A., Andersen, K.K., Bigler, M., Clausen, H.B., Dahl-Jensen, D., Davies, S.M., Johnsen, S.J., Muscheler, R., Rasmussen, S.O., Röthlisberger, R., Steffensen, J.P., Vinther, B., 2006. The Greenland Ice Core Chronology 2005, 15–42ka. Part 2: comparison to other records. Quat. Sci. Rev. 25, 3258–3267. https://doi.org/10.1016/j.quascirev.2006.08.003.

Svensson, A., Andersen, K.K., Bigler, M., Clausen, H.B., Dahl-Jensen, D., Davies, S.M., Johnsen, S.J., Muscheler, R., Parrenin, F., Rasmussen, S.O., Röthlisberger, R.,

Seierstad, I., Steffensen, J.P., Vinther, B.M., 2008. A 60 000 year Greenland stratigraphic ice core chronology. Clim. Past 4, 47–57. https://doi.org/10.5194/cp-4-47-2008.

Svensson, A., Dahl-Jensen, D., Steffensen, J.P., Blunier, T., Rasmussen, S.O., Vinther, B.M., Vallelonga, P., Capron, E., Gkinis, V., Cook, E., Kjær, H.A., Muscheler, R., Kipfstuhl, S., Wilhelms, F., Stocker, T.F., Fischer, H., Adolphi, F., Erhardt, T., Sigl, M., Landais, A., Parrenin, F., Buizert, C., McConnell, J.R., Severi, M., Mulvaney, R., Bigler, M., 2020. Bipolar volcanic synchronization of abrupt climate change in Greenland and Antarctic ice cores during the last glacial period. Clim. Past 16, 1565–1580. https://doi.org/10.5194/cp-16-1565-2020.

Svensson, A., Bigler, M., Blunier, T., Clausen, H.B., Dahl-Jensen, D., Fischer, H., Fujita, S., Goto-Azuma, K., Johnsen, S.J., Kawamura, K., Kipfstuhl, S., Kohno, M., Parrenin, F., Popp, T., Rasmussen, S.O., Schwander, J., Seierstad, I., Severi, M., Steffensen, J.P., Udisti, R., Uemura, R., Vallelonga, P., Vinther, B.M., Wegner, A., Wilhelms, F., Winstrup, M., 2013. Direct linking of Greenland and Antarctic ice cores at the Toba eruption (74 ka BP). Clim. Past 9, 749–766. https://doi.org/10.5194/cp-9-749-2013.

Takahashi, S., Kameda, T., Enomoto, H., Motoyama, H., Watanabe, O., 2004. Automatic weather station (AWS) data collected by the 33rd to 42nd Japanese antarctic Research expeditions during 1993-2001, JARE data reports. Meteorology 36, 1–416. https://doi.org/10.15094/00005871.

Uemura, R., Motoyama, H., Masson-Delmotte, V., Jouzel, J., Kawamura, K., Goto-Azuma, K., Fujita, S., Kuramoto, T., Hirabayashi, M., Miyake, T., Ohno, H., Fujita, K., Abe-Ouchi, A., Iizuka, Y., Horikawa, S., Igarashi, M., Suzuki, K., Suzuki, T., Fujii, Y., 2018. Asynchrony between Antarctic temperature and CO_2 associated with obliquity over the past 720,000 years. Nat. Commun. 9. https://doi.org/10.1038/s41467-018-03328-3.

Veres, D., Bazin, L., Landais, A., Toyé Mahamadou Kele, H., Lemieux-Dudon, B., Parrenin, F., Martinerie, P., Blayo, E., Blunier, T., Capron, E., Chappellaz, J., Rasmussen, S.O., Severi, M., Svensson, A., Vinther, B., Wolff, E.W., 2013. The Antarctic ice core chronology (AICC2012): an optimized multi-parameter and multi-site dating approach for the last 120 thousand years. Clim. Past 9, 1733–1748. https://doi.org/10.5194/cp-9-1733-2013.

Vinther, B.M., Clausen, H.B., Johnsen, S.J., Rasmussen, S.O., Andersen, K.K., Buchardt, S.L., Dahl-Jensen, D., Seierstad, I.K., Siggaard-Andersen, M.L., Steffensen, J.P., Svensson, A., Olsen, J., Heinemeier, J., 2006. A synchronized dating of three Greenland ice cores throughout the Holocene. J. Geophys. Res.: Atmosphere 111. https://doi.org/10.1029/2005JD006921.

Waelbroeck, C., Jouzel, J., Labeyrie, L., Lorius, C., Labracherie, M., Stievenard, M., Barkov, N.I., 1995. A comparison of the Vostok ice deuterium record and series from Southern Ocean core MD 88-770 over the last two glacial-interglacial cycles. Clim. Dynam. 12, 113–123. https://doi.org/10.1007/BF00223724.

Wang, Y., Cheng, H., Edwards, R.L., Kong, X., Shao, X., Chen, S., Wu, J., Jiang, X., Wang, X., An, Z., 2008. Millennial- and orbital-scale changes in the East Asian monsoon over the past 224,000 years. Nature 451, 1090–1093. https://doi.org/10.1038/nature06692.

Wang, Y.J., Cheng, H., Lawrence Edwards, R., An, Z.S., Wu, J.Y., Shen, C.C., Dorale, J.A., 2001. A high-resolution absolute-dated late pleistocene monsoon record from Hulu cave, China. Science 294, 2345–2348. https://doi.org/10.1126/science.1064618.

Watanabe, O., Shoji, H., Fujii, Y., Narita, H., Aoki, S., 2003a. Dating of the Dome Fuji, Antarctica deep ice core. Mem. Nat. Inst. Polar Res. 25–37.

Watanabe, O., Jouzel, J., Johnsen, S., Parrenin, F., Shoji, H., Yoshida, N., 2003b. Homogeneous climate variability across East Antarctica over the past three glacial cycles. Nature 422, 509–512. https://doi.org/10.1038/nature01525.

Wendt, K.A., Li, X., Edwards, R.L., Cheng, H., Spötl, C., 2021. Precise timing of MIS 7 substages from the Austrian Alps. Clim. Past 17, 1443–1454. https://doi.org/10.5194/cp-17-1443-2021.

Wolff, E.W., Chappellaz, J., Blunier, T., Rasmussen, S.O., Svensson, A., 2010. Millennial-scale variability during the last glacial: the ice core record. Quat. Sci. Rev. 29, 2828–2838. https://doi.org/10.1016/j.quascirev.2009.10.013.